

# Recursive anisotropy: a spatial taphonomic study of the Early Pleistocene vertebrate assemblage of Tsiotra Vryssi, Mygdonia Basin, Greece

D. Giusti<sup>a,\*</sup>, G. E. Konidaris<sup>a</sup>, V. Tourloukis<sup>a</sup>, M. Marini<sup>b</sup>, M. Maron<sup>b</sup>, A. Zerboni<sup>b</sup>, N. Thompson<sup>a</sup>, G. D. Koufos<sup>c</sup>,  
D. S. Kostopoulos<sup>c</sup>, K. Harvati<sup>a</sup>

<sup>a</sup>*Paläoanthropologie, Senckenberg Centre for Human Evolution and Palaeoenvironment, Eberhard Karls Universität Tübingen, Rümelinstr. 23, 72070 Tübingen, Germany*

<sup>b</sup>*Università degli Studi di Milano, via Mangiagalli 34, 20133 Milano, Italy*

<sup>c</sup>*Aristotle University of Thessaloniki, Department of Geology, Laboratory of Geology and Palaeontology, 54124 Thessaloniki, Greece*

## Abstract

By applying advanced spatial statistical methods, spatial taphonomy complements the traditional taphonomic approach and enhances our understanding of biostratinomic and diagenetic processes. In this study, we elaborate on a specific aspect - spatial anisotropy - of taphonomic processes. We aim to unravel the taphonomic history of the Early Pleistocene vertebrate assemblage of Tsiotra Vryssi (Mygdonia Basin, Macedonia, Greece). Circular statistics are used for the fabric analysis of elongated elements; geostatistics (directional variograms), wavelet and point pattern analyses are applied for detecting anisotropy at the assemblage level. The anisotropy of magnetic susceptibility (AMS) of sedimentary magnetic minerals is as well investigated. The results of our analyses, integrated with preliminary remarks about the differential preservation of skeletal elements, sedimentological and micro-morphological observations, suggest multiple dispersion events and recurrent spatial re-arrangement of a lag, (peri)autochthonous assemblage, consistent with the cyclical lateral switching of a braided fluvial system. Furthermore, this study offers an important contribution to the building of a spatial taphonomic referential framework for the interpretation of other fossil vertebrate assemblages, including archaeo-palaeontological ones.

**Keywords:** Anisotropy, Spatial taphonomy, Taphonomy, Site formation processes, Early Pleistocene, Greece

## 1. Introduction

Since the first definition of taphonomy as “the study of the transition (in all its details) of animal remains from the biosphere into the lithosphere” (Efremov, 1940), the spatial properties of taphonomic processes received special attention. Concerned about thanatocoenosis, Efremov (1940) indicated as chief part of a taphonomic study, among others, the analysis of “the spatial distribution of animal remains and their distribution relatively to the planes of stratification”. More recent research on early hominid evolution (Behrensmeyer, 1975a; Boaz and Behrensmeyer, 1976; Hill, 1976) extended the original definition of taphonomy beyond its role as a “new branch of paleontology” (Efremov, 1940) to include also formation and modification processes of the archaeological record. Despite some misrepresentations in the archaeological adaptation of the original concept (e.g., the ontological difference between natural and cultural formation processes; Domínguez-Rodrigo et al., 2011; Lyman, 2010), in the last decades taphonomy has widened its theoretical and methodological framework towards an integrative and multidisciplinary investigation that aims to reconstruct the past in all its details, incorporating any signal of the processes, both natural and cultural, that modified the original prop-

erties of the organic and inorganic components (Domínguez-Rodrigo et al., 2011).

If taphonomy evolved towards an evolutionary and systemic approach that embraces multiple taphonomic levels of organisation (i.e., basic taphonomic elements, taphonomic groups [taphons], taphonomic populations and taphoclades; Fernández-López, 2006), likewise, the study of the spatial properties of taphonomic processes extended from the analysis of the spatial distribution of animal remains in relation to the stratigraphic setting, towards a multilevel quantitative investigation of the spatial behaviour of different taphonomic entities (*sensu* Fernández-López, 2006). Therefore, spatial taphonomy (Domínguez-Rodrigo et al., 2017; Giusti and Arzarello, 2016), encompasses the spatial properties of basic entities (i.e., taphonomic elements, constituting the fossil record), as well as higher level entities (e.g., taphonomic groups or populations). Indeed, at multiple scales and levels of organisation, the spatial patterns observed in any palaeontological or archaeological assemblage retain valuable information about taphonomic accumulation and re-elaboration processes (*sensu* Fernández-López et al., 2002). Spatial taphonomic data, appropriately recorded, can be quantitatively analysed within a statistical framework in order to reliably draw inferences about taphonomic processes, in turn with consequences for palaeoecological reconstructions (Fernández-Jalvo et al., 2011), biochronological estimates and the interpretation of past human behaviours.

\*Corresponding author

Email address: domenico.giusti@uni-tuebingen.de (D. Giusti)

In this study, we elaborate on a specific aspect - anisotropy<sup>106</sup> - of the spatial properties of taphonomic entities, with implications<sup>107</sup> for the interpretation of taphonomic processes. Anisotropy<sup>108</sup> as opposed to isotropy, is generally defined as the property of<sup>109</sup> a process of being directionally dependent. Spatial anisotropic<sup>110</sup> patterns can be seen as products of physical anisotropic processes,<sup>111</sup> such as fluvial or eolian processes, which modified at multiple scales and levels of organisation the original spatial<sup>112</sup> properties of taphonomic entities.

At the level of basic taphonomic elements, anisotropy, expressed<sup>113</sup> as preferential orientation of fossils or artefacts, is among<sup>114</sup> the key variables used for interpreting site formation and modification<sup>115</sup> processes. Especially in terrestrial alluvial environments,<sup>116</sup> anisotropy is one of the proxies traditionally used to discriminate<sup>117</sup> autochthonous vs. allochthonous assemblages (Petraglia and Nash,<sup>118</sup> 1987; Petraglia and Potts,<sup>119</sup> 1994; Schick,<sup>120</sup> 1987; Toots,<sup>121</sup> 1965; Voorhies,<sup>122</sup> 1969, among others). The orientation of elongated<sup>123</sup> elements, prone to preferentially align along the flow<sup>124</sup> direction, would eventually indicate the action of water-flows<sup>125</sup> and suggest substantial transport prior to burial. Nevertheless,<sup>126</sup> anisotropy has been equally documented in autochthonous assemblages<sup>127</sup> subjected to low-energy water-flows (Cobo-Sánchez,<sup>128</sup> 2014; Domínguez-Rodrigo et al.,<sup>129</sup> 2012, 2014d); hence,<sup>130</sup> it can be a necessary but not sufficient condition to differentiate<sup>131</sup> allochthony from autochthony (Lenoble and Bertran,<sup>132</sup> 2004). Moreover,<sup>133</sup> besides water-flow processes, anisotropy has been<sup>134</sup> as well observed in association with a wide range of other biotrinomic<sup>135</sup> processes, such as slope processes (Bertran and Texier,<sup>136</sup> 1995) and trampling (Benito-Calvo et al.,<sup>137</sup> 2011).

Although the anisotropy of basic taphonomic elements have<sup>138</sup> been long studied, the anisotropy of higher level taphonomic<sup>139</sup> entities received by far less attention (see Markofsky and Bevan,<sup>140</sup> 2012 for a directional analysis of archaeological surface<sup>141</sup> distributions). Here we address this research gap and conduct a<sup>142</sup> spatial taphonomic study of anisotropy both at the level of fossil<sup>143</sup> specimens and at the assemblage level. The present study<sup>144</sup> uses a comprehensive set of spatial statistics (fabric analysis,<sup>145</sup> geostatistics, wavelet analysis, point pattern analysis) in order<sup>146</sup> to identify directional trends that may not be readily apparent.<sup>147</sup> Indeed, beyond the traditional approach of eye-spotting spatial<sup>148</sup> patterns, spatial statistics allow one to adopt a more formal,<sup>149</sup> quantitative approach.

Furthermore, at the scale of sedimentary particles, anisotropy<sup>146</sup> is investigated by means of anisotropy of magnetic susceptibility<sup>147</sup> (AMS). AMS refers to the property of elongated magnetic<sup>148</sup> crystals to orient parallel to the flow direction when transported<sup>149</sup> as sedimentary clasts. In sedimentology, AMS analysis<sup>150</sup> is widely applied in order to determine paleoflows in a range<sup>151</sup> of depositional environments, including turbidite systems, contouritic drifts, beaches, deltas and tidal flats (Felletti et al.,<sup>152</sup> 2016; Liu et al.,<sup>153</sup> 2001; Lowrie and Hirt,<sup>154</sup> 1987; Novak et al.,<sup>155</sup> 2014; Parés et al.,<sup>156</sup> 2007, among others).

Therefore, integrating the results of our multiscale and multilevel analysis of anisotropy with preliminary remarks about differential taphonomic preservation, sedimentological and micromorphological observations, we aim to disentangle the taphonomic history of the fossiliferous locality Tsiotra Vryssi (Myg-

donia Basin, Macedonia, Greece; Konidaris et al., 2015).

Finally, this study offers an important contribution to the building of a spatial taphonomic referential framework for the interpretation of other fossil vertebrate assemblages, including archaeo-palaeontological ones (Domínguez-Rodrigo et al., 2017).

## 2. The palaeontological site of Tsiotra Vryssi (TSR)

Tsiotra Vryssi (TSR) is located in the Mygdonia Basin (Macedonia, Greece), about 45 km Southeast of Thessaloniki (Fig. 1). TSR was discovered in 2014 by a joint research team from the Aristotle University of Thessaloniki and the Eberhard Karls University of Tübingen during systematic field surveys in the basin. After the first collection of fossils from the exposed natural section and the test excavation carried out in 2014, systematic excavation of the site took place in 2015 and is still ongoing (Fig. 2a).

To date, the excavation covers about a 10 m-thick stratigraphic interval from the upper Gerakarou Formation (Fig. 1), a suite of continental clastic deposits of mainly fluvial origin and inter-layered paleosols (Konidaris et al., 2015; Koufos et al., 1995). The TSR fauna occurs mainly within a c. 1 m-thick interval of silts (uppermost part of unit Geo2, see Fig 3) and comprises several mammalian taxa, as well as some birds and reptiles, whose preliminary biochronological correlation is consistent with a late Villafranchian (Early Pleistocene) age (Konidaris et al., 2016, 2015).

Two main depositional units are identified (Geo 1 and Geo 2, from younger to older; Fig. 3). The fossiliferous unit Geo 2 begins with ~1.5 m (Geo 2b in Fig. 3) of cross-stratified gravelly sands organised into dm-thick beds with a range of planar to trough-cross laminations. Noteworthy, Geo 2b can be followed laterally for at least 150m in the E-W direction, suggesting an extensive setting of deposition. Above a sharp contact, a few tens of cm of well-sorted, structure-less fine sands follow, which rapidly grade upward into the deposit forming the matrix of the main TSR fossil assemblage (Geo 2a in Fig. 3). This is represented by ~1 m of poorly sorted silts (moderately rich in mica grains), locally intercalated by cm-thick lenses of medium-coarse grained sands and relatively more clayey in the uppermost 30 cm of the deposit. Apart for alignment of isolated sand to granule grade clasts and some crude parallel lamination in coarse lenses, the deposits appear overall structureless. Typically, Geo 2a has a very pale brown colour with a few (less than 10%) pink to reddish yellow mottles, whereas the topmost part of Geo 2a has a strong brown to dark yellowish brown matrix with about the 15-20% of reddish yellow mottles. This change in colour is associated with the occurrence of very small calcareous nodules and common to abundant Mn-Fe-bearing nodules with diameter less than 1 cm (see micromorphological analysis in Section 4.5).

Geo 1b is represented by an up to 2 m-thick bed set of cross-stratified gravelly sands and gravels, similar to those observed in Geo 2b (Fig. 3). It sits on top of a basal erosion, down-cutting deeply into older sediments (Geo 2a) and shallowing toward the West. In the same direction, the Geo 1b beds tend

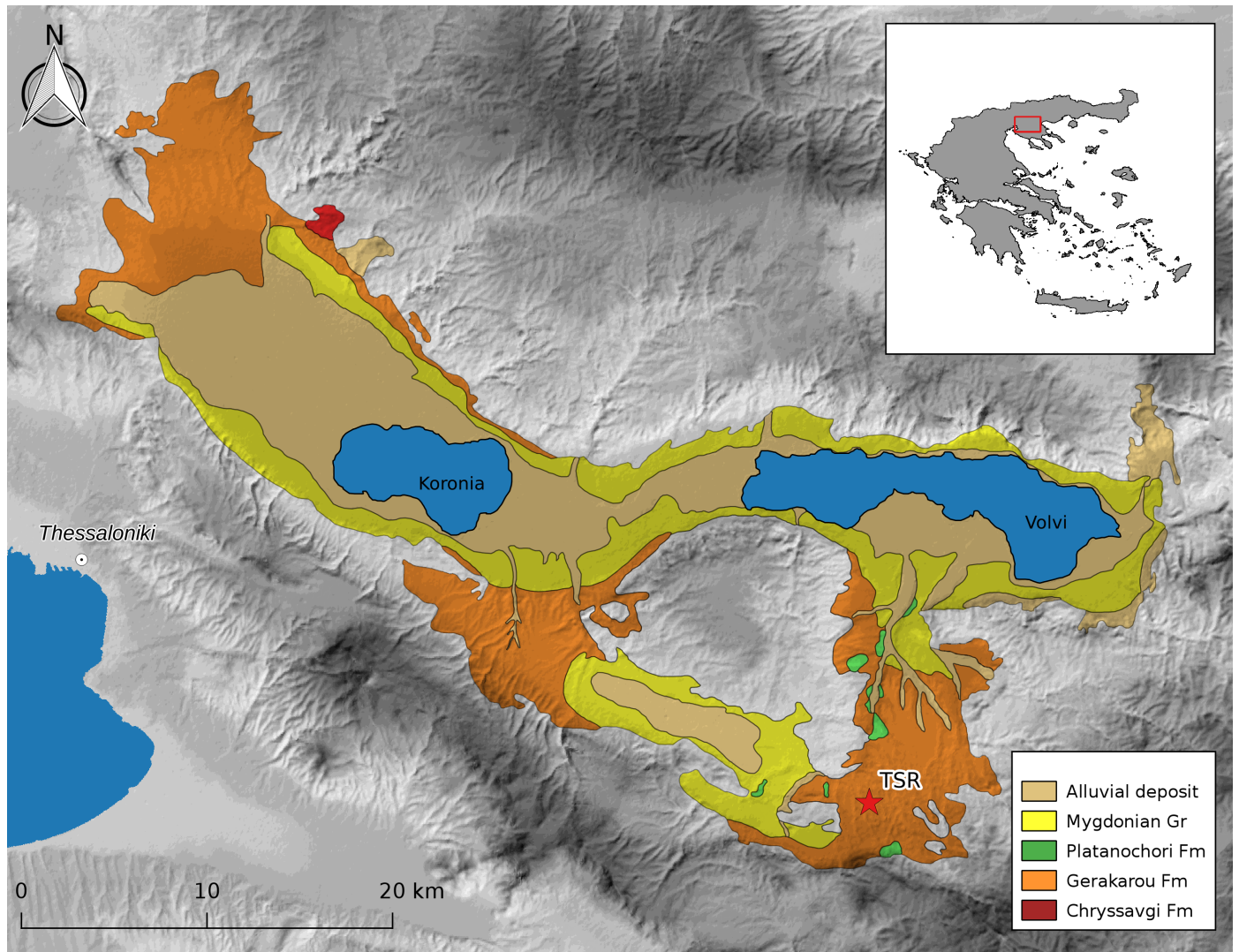


Figure 1: Geological setting of the Mygdonia Basin (Macedonia, Greece) showing the Neogene and Quaternary lithostratigraphic units and the location of Tsio-tra Vryssi (TSR), modified after [Koufos et al. \(1995\)](#)

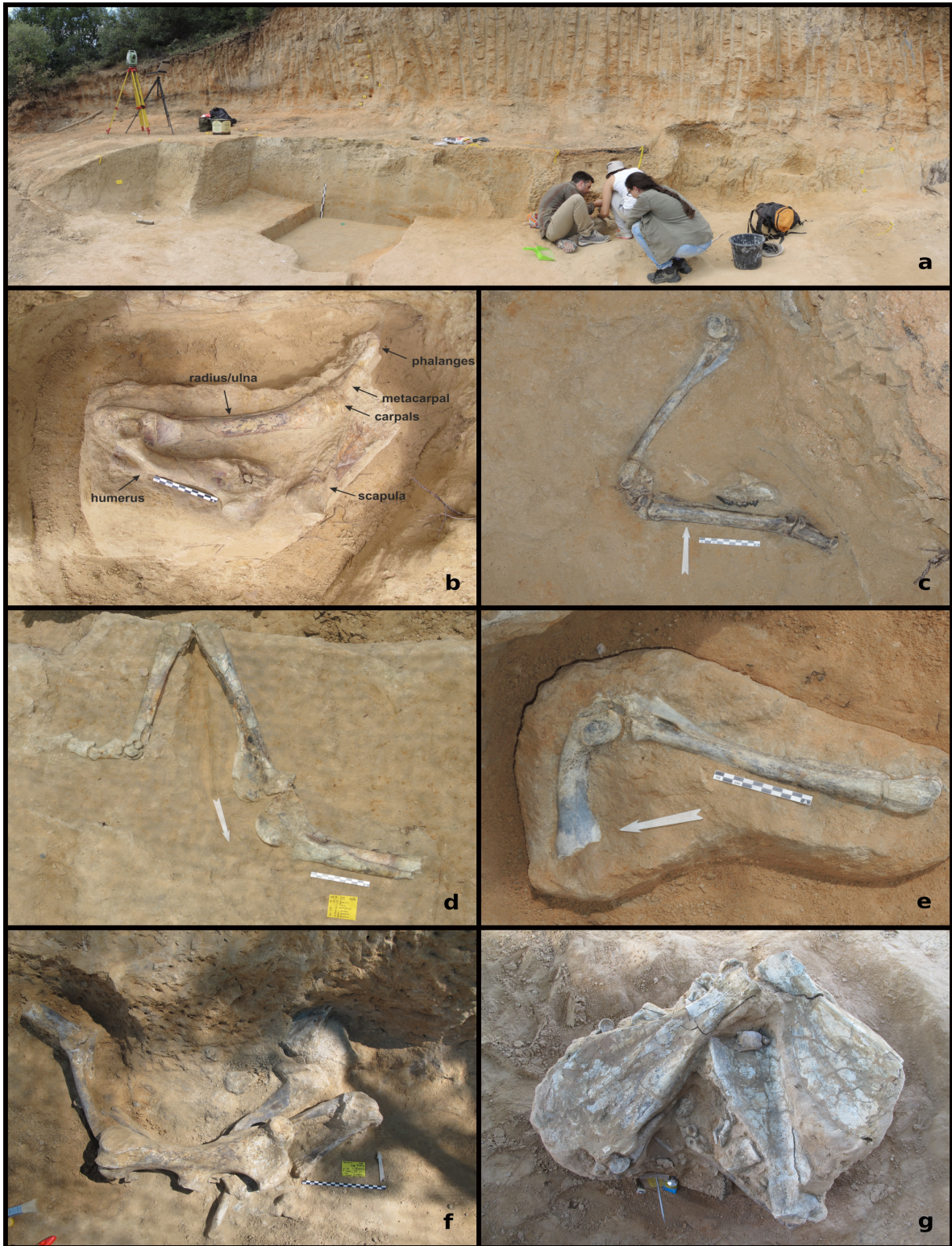


Figure 2: Panoramic view (2017) of the excavation area of Tsikota Vryssi. Pictures of articulated specimens (a, b, c, d) and clusters of bones (e, f).

160 to be thinner, finer grained a  
161 ing less energetic hydrodyna  
162 posed, the younger Geo 1a  
163 m-thick section of poorly sil  
164 tions, which rapidly grades i  
165 brown colour.

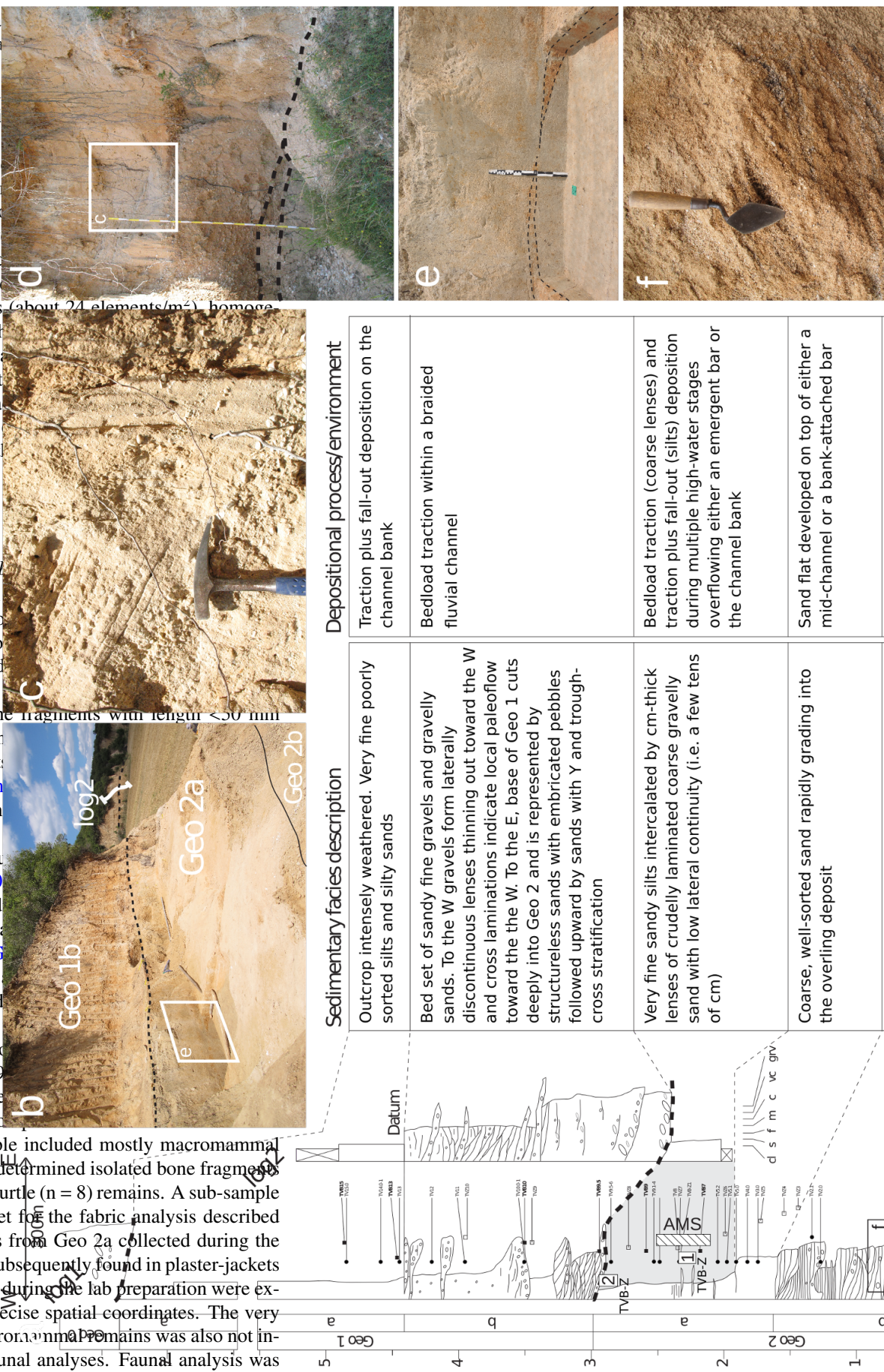
Overall, the stratigraphic  
166  
167  
168  
169  
170  
171  
172  
173  
174  
175  
176  
177  
178  
179  
180  
181  
182  
183  
184  
185  
186  
187  
188  
189  
190  
191  
192  
193  
194  
195  
196  
197  
198  
199  
200  
201  
202  
203  
204  
205  
206  
207  
208  
209  
210  
211  
212  
213  
214  
215  
216  
217  
218  
219  
220  
221  
222  
223  
224  
225  
226  
227  
228  
229  
230  
231  
232  
233  
234  
235  
236  
237  
238  
239  
240  
241  
242  
243  
244  
245  
246  
247  
248  
249  
250  
251  
252  
253  
254  
255  
256  
257  
258  
259  
260  
261  
262  
263  
264  
265  
266  
267  
268  
269  
270  
271  
272  
273  
274  
275  
276  
277  
278  
279  
280  
281  
282  
283  
284  
285  
286  
287  
288  
289  
290  
291  
292  
293  
294  
295  
296  
297  
298  
299  
300  
301  
302  
303  
304  
305  
306  
307  
308  
309  
310  
311  
312  
313  
314  
315  
316  
317  
318  
319  
320  
321  
322  
323  
324  
325  
326  
327  
328  
329  
330  
331  
332  
333  
334  
335  
336  
337  
338  
339  
340  
341  
342  
343  
344  
345  
346  
347  
348  
349  
350  
351  
352  
353  
354  
355  
356  
357  
358  
359  
360  
361  
362  
363  
364  
365  
366  
367  
368  
369  
370  
371  
372  
373  
374  
375  
376  
377  
378  
379  
380  
381  
382  
383  
384  
385  
386  
387  
388  
389  
390  
391  
392  
393  
394  
395  
396  
397  
398  
399  
400  
401  
402  
403  
404  
405  
406  
407  
408  
409  
410  
411  
412  
413  
414  
415  
416  
417  
418  
419  
420  
421  
422  
423  
424  
425  
426  
427  
428  
429  
430  
431  
432  
433  
434  
435  
436  
437  
438  
439  
440  
441  
442  
443  
444  
445  
446  
447  
448  
449  
450  
451  
452  
453  
454  
455  
456  
457  
458  
459  
460  
461  
462  
463  
464  
465  
466  
467  
468  
469  
470  
471  
472  
473  
474  
475  
476  
477  
478  
479  
480  
481  
482  
483  
484  
485  
486  
487  
488  
489  
490  
491  
492  
493  
494  
495  
496  
497  
498  
499  
500  
501  
502  
503  
504  
505  
506  
507  
508  
509  
510  
511  
512  
513  
514  
515  
516  
517  
518  
519  
520  
521  
522  
523  
524  
525  
526  
527  
528  
529  
530  
531  
532  
533  
534  
535  
536  
537  
538  
539  
540  
541  
542  
543  
544  
545  
546  
547  
548  
549  
550  
551  
552  
553  
554  
555  
556  
557  
558  
559  
559  
560  
561  
562  
563  
564  
565  
566  
567  
568  
569  
569  
570  
571  
572  
573  
574  
575  
576  
577  
578  
579  
579  
580  
581  
582  
583  
584  
585  
586  
587  
588  
589  
589  
590  
591  
592  
593  
594  
595  
596  
597  
598  
599  
599  
600  
601  
602  
603  
604  
605  
606  
607  
608  
609  
609  
610  
611  
612  
613  
614  
615  
616  
617  
618  
619  
619  
620  
621  
622  
623  
624  
625  
626  
627  
628  
629  
629  
630  
631  
632  
633  
634  
635  
636  
637  
638  
639  
639  
640  
641  
642  
643  
644  
645  
646  
647  
648  
649  
649  
650  
651  
652  
653  
654  
655  
656  
657  
658  
659  
659  
660  
661  
662  
663  
664  
665  
666  
667  
668  
669  
669  
670  
671  
672  
673  
674  
675  
676  
677  
678  
679  
679  
680  
681  
682  
683  
684  
685  
686  
687  
688  
689  
689  
690  
691  
692  
693  
694  
695  
696  
697  
698  
699  
699  
700  
701  
702  
703  
704  
705  
706  
707  
708  
709  
709  
710  
711  
712  
713  
714  
715  
716  
717  
718  
719  
719  
720  
721  
722  
723  
724  
725  
726  
727  
728  
729  
729  
730  
731  
732  
733  
734  
735  
736  
737  
738  
739  
739  
740  
741  
742  
743  
744  
745  
746  
747  
748  
749  
749  
750  
751  
752  
753  
754  
755  
756  
757  
758  
759  
759  
760  
761  
762  
763  
764  
765  
766  
767  
768  
769  
769  
770  
771  
772  
773  
774  
775  
776  
777  
778  
779  
779  
780  
781  
782  
783  
784  
785  
786  
787  
788  
789  
789  
790  
791  
792  
793  
794  
795  
796  
797  
798  
799  
799  
800  
801  
802  
803  
804  
805  
806  
807  
808  
809  
809  
810  
811  
812  
813  
814  
815  
816  
817  
818  
819  
819  
820  
821  
822  
823  
824  
825  
826  
827  
828  
829  
829  
830  
831  
832  
833  
834  
835  
836  
837  
838  
839  
839  
840  
841  
842  
843  
844  
845  
846  
847  
848  
849  
849  
850  
851  
852  
853  
854  
855  
856  
857  
858  
859  
859  
860  
861  
862  
863  
864  
865  
866  
867  
868  
869  
869  
870  
871  
872  
873  
874  
875  
876  
877  
878  
879  
879  
880  
881  
882  
883  
884  
885  
886  
887  
888  
889  
889  
890  
891  
892  
893  
894  
895  
896  
897  
898  
899  
899  
900  
901  
902  
903  
904  
905  
906  
907  
908  
909  
909  
910  
911  
912  
913  
914  
915  
916  
917  
918  
919  
919  
920  
921  
922  
923  
924  
925  
926  
927  
928  
929  
929  
930  
931  
932  
933  
934  
935  
936  
937  
938  
939  
939  
940  
941  
942  
943  
944  
945  
946  
947  
948  
949  
949  
950  
951  
952  
953  
954  
955  
956  
957  
958  
959  
959  
960  
961  
962  
963  
964  
965  
966  
967  
968  
969  
969  
970  
971  
972  
973  
974  
975  
976  
977  
978  
979  
979  
980  
981  
982  
983  
984  
985  
986  
987  
988  
989  
989  
990  
991  
992  
993  
994  
995  
996  
997  
998  
999  
999  
1000  
1001  
1002  
1003  
1004  
1005  
1006  
1007  
1008  
1009  
1009  
1010  
1011  
1012  
1013  
1014  
1015  
1016  
1017  
1018  
1019  
1019  
1020  
1021  
1022  
1023  
1024  
1025  
1026  
1027  
1028  
1029  
1029  
1030  
1031  
1032  
1033  
1034  
1035  
1036  
1037  
1038  
1039  
1039  
1040  
1041  
1042  
1043  
1044  
1045  
1046  
1047  
1048  
1049  
1049  
1050  
1051  
1052  
1053  
1054  
1055  
1056  
1057  
1058  
1059  
1059  
1060  
1061  
1062  
1063  
1064  
1065  
1066  
1067  
1068  
1069  
1069  
1070  
1071  
1072  
1073  
1074  
1075  
1076  
1077  
1078  
1079  
1079  
1080  
1081  
1082  
1083  
1084  
1085  
1086  
1087  
1088  
1089  
1089  
1090  
1091  
1092  
1093  
1094  
1095  
1096  
1097  
1098  
1099  
1099  
1100  
1101  
1102  
1103  
1104  
1105  
1106  
1107  
1108  
1109  
1109  
1110  
1111  
1112  
1113  
1114  
1115  
1116  
1117  
1118  
1119  
1119  
1120  
1121  
1122  
1123  
1124  
1125  
1126  
1127  
1128  
1129  
1129  
1130  
1131  
1132  
1133  
1134  
1135  
1136  
1137  
1138  
1139  
1139  
1140  
1141  
1142  
1143  
1144  
1145  
1146  
1147  
1148  
1149  
1149  
1150  
1151  
1152  
1153  
1154  
1155  
1156  
1157  
1158  
1159  
1159  
1160  
1161  
1162  
1163  
1164  
1165  
1166  
1167  
1168  
1169  
1169  
1170  
1171  
1172  
1173  
1174  
1175  
1176  
1177  
1178  
1179  
1179  
1180  
1181  
1182  
1183  
1184  
1185  
1186  
1187  
1188  
1189  
1189  
1190  
1191  
1192  
1193  
1194  
1195  
1196  
1197  
1198  
1199  
1199  
1200  
1201  
1202  
1203  
1204  
1205  
1206  
1207  
1208  
1209  
1209  
1210  
1211  
1212  
1213  
1214  
1215  
1216  
1217  
1218  
1219  
1219  
1220  
1221  
1222  
1223  
1224  
1225  
1226  
1227  
1228  
1229  
1229  
1230  
1231  
1232  
1233  
1234  
1235  
1236  
1237  
1238  
1239  
1239  
1240  
1241  
1242  
1243  
1244  
1245  
1246  
1247  
1248  
1249  
1249  
1250  
1251  
1252  
1253  
1254  
1255  
1256  
1257  
1258  
1259  
1259  
1260  
1261  
1262  
1263  
1264  
1265  
1266  
1267  
1268  
1269  
1269  
1270  
1271  
1272  
1273  
1274  
1275  
1276  
1277  
1278  
1279  
1279  
1280  
1281  
1282  
1283  
1284  
1285  
1286  
1287  
1288  
1289  
1289  
1290  
1291  
1292  
1293  
1294  
1295  
1296  
1297  
1298  
1299  
1299  
1300  
1301  
1302  
1303  
1304  
1305  
1306  
1307  
1308  
1309  
1309  
1310  
1311  
1312  
1313  
1314  
1315  
1316  
1317  
1318  
1319  
1319  
1320  
1321  
1322  
1323  
1324  
1325  
1326  
1327  
1328  
1329  
1329  
1330  
1331  
1332  
1333  
1334  
1335  
1336  
1337  
1338  
1339  
1339  
1340  
1341  
1342  
1343  
1344  
1345  
1346  
1347  
1348  
1349  
1349  
1350  
1351  
1352  
1353  
1354  
1355  
1356  
1357  
1358  
1359  
1359  
1360  
1361  
1362  
1363  
1364  
1365  
1366  
1367  
1368  
1369  
1369  
1370  
1371  
1372  
1373  
1374  
1375  
1376  
1377  
1378  
1379  
1379  
1380  
1381  
1382  
1383  
1384  
1385  
1386  
1387  
1388  
1389  
1389  
1390  
1391  
1392  
1393  
1394  
1395  
1396  
1397  
1398  
1399  
1399  
1400  
1401  
1402  
1403  
1404  
1405  
1406  
1407  
1408  
1409  
1409  
1410  
1411  
1412  
1413  
1414  
1415  
1416  
1417  
1418  
1419  
1419  
1420  
1421  
1422  
1423  
1424  
1425  
1426  
1427  
1428  
1429  
1429  
1430  
1431  
1432  
1433  
1434  
1435  
1436  
1437  
1438  
1439  
1439  
1440  
1441  
1442  
1443  
1444  
1445  
1446  
1447  
1448  
1449  
1449  
1450  
1451  
1452  
1453  
1454  
1455  
1456  
1457  
1458  
1459  
1459  
1460  
1461  
1462  
1463  
1464  
1465  
1466  
1467  
1468  
1469  
1469  
1470  
1471  
1472  
1473  
1474  
1475  
1476  
1477  
1478  
1479  
1479  
1480  
1481  
1482  
1483  
1484  
1485  
1486  
1487  
1488  
1489  
1489  
1490  
1491  
1492  
1493  
1494  
1495  
1496  
1497  
1498  
1499  
1499  
1500  
1501  
1502  
1503  
1504  
1505  
1506  
1507  
1508  
1509  
1509  
1510  
1511  
1512  
1513  
1514  
1515  
1516  
1517  
1518  
1519  
1519  
1520  
1521  
1522  
1523  
1524  
1525  
1526  
1527  
1528  
1529  
1529  
1530  
1531  
1532  
1533  
1534  
1535  
1536  
1537  
1538  
1539  
1539  
1540  
1541  
1542  
1543  
1544  
1545  
1546  
1547  
1548  
1549  
1549  
1550  
1551  
1552  
1553  
1554  
1555  
1556  
1557  
1558  
1559  
1559  
1560  
1561  
1562  
1563  
1564  
1565  
1566  
1567  
1568  
1569  
1569  
1570  
1571  
1572  
1573  
1574  
1575  
1576  
1577  
1578  
1579  
1579  
1580  
1581  
1582  
1583  
1584  
1585  
1586  
1587  
1588  
1589  
1589  
1590  
1591  
1592  
1593  
1594  
1595  
1596  
1597  
1598  
1599  
1599  
1600  
1601  
1602  
1603  
1604  
1605  
1606  
1607  
1608  
1609  
1609  
1610  
1611  
1612  
1613  
1614  
1615  
1616  
1617  
1618  
1619  
1619  
1620  
1621  
1622  
1623  
1624  
1625  
1626  
1627  
1628  
1629  
1629  
1630  
1631  
1632  
1633  
1634  
1635  
1636  
1637  
1638  
1639  
1639  
1640  
1641  
1642  
1643  
1644  
1645  
1646  
1647  
1648  
1649  
1649  
1650  
1651  
1652  
1653  
1654  
1655  
1656  
1657  
1658  
1659  
1659  
1660  
1661  
1662  
1663  
1664  
1665  
1666  
1667  
1668  
1669  
1669  
1670  
1671  
1672  
1673  
1674  
1675  
1676  
1677  
1678  
1679  
1679  
1680  
1681  
1682  
1683  
1684  
1685  
1686  
1687  
1688  
1689  
1689  
1690  
1691  
1692  
1693  
1694  
1695  
1696  
1697  
1698  
1699  
1699  
1700  
1701  
1702  
1703  
1704  
1705  
1706  
1707  
1708  
1709  
1709  
1710  
1711  
1712  
1713  
1714  
1715  
1716  
1717  
1718  
1719  
1719  
1720  
1721  
1722  
1723  
1724  
1725  
1726  
1727  
1728  
1729  
1729  
1730  
1731  
1732  
1733  
1734  
1735  
1736  
1737  
1738  
1739  
1739  
1740  
1741  
1742  
1743  
1744  
1745  
1746  
1747  
1748  
1749  
1749  
1750  
1751  
1752  
1753  
1754  
1755  
1756  
1757  
1758  
1759  
1759  
1760  
1761  
1762  
1763  
1764  
1765  
1766  
1767  
1768  
1769  
1769  
1770  
1771  
1772  
1773  
1774  
1775  
1776  
1777  
1778  
1779  
1779  
1780  
1781  
1782  
1783  
1784  
1785  
1786  
1787  
1788  
1789  
1789  
1790  
1791  
1792  
1793  
1794  
1795  
1796  
1797  
1798  
1799  
1799  
1800  
1801  
1802  
1803  
1804  
1805  
1806  
1807  
1808  
1809  
1809  
1810  
1811  
1812  
1813  
1814  
1815  
1816  
1817  
1818  
1819  
1819  
1820  
1821  
1822  
1823  
1824  
1825  
1826  
1827  
1828  
1829  
1829  
1830  
1831  
1832  
1833  
1834  
1835  
1836  
1837  
1838  
1839  
1839  
1840  
1841  
1842  
1843  
1844  
1845  
1846  
1847  
1848  
1849  
1849  
1850  
1851  
1852  
1853  
1854  
1855  
1856  
1857  
1858  
1859  
1859  
1860  
1861  
1862  
1863  
1864  
1865  
1866  
1867  
1868  
1869  
1869  
1870  
1871  
1872  
1873  
1874  
1875  
1876  
1877  
1878  
1879  
1879  
1880  
1881  
1882  
1883  
1884  
1885  
1886  
1887  
1888  
1889  
1889  
1890  
1891  
1892  
1893  
1894  
1895  
1896  
1897  
1898  
1899  
1899  
1900  
1901  
1902  
1903  
1904  
1905  
1906  
1907  
1908  
1909  
1909  
1910  
1911  
1912  
1913  
1914  
1915  
1916  
1917  
1918  
1919  
1919  
1920  
1921  
1922  
1923  
1924  
1925  
1926  
1927  
1928  
1929  
1929  
1930  
1931  
1932  
1933  
1934  
1935  
1936  
1937  
1938  
1939  
1939  
1940  
1941  
1942  
1943  
1944  
1945  
1946  
1947  
1948  
1949  
1949  
1950  
1951  
1952  
1953  
1954  
1955  
1956  
1957  
1958  
1959  
1959  
1960  
1961  
1962  
1963  
1964  
1965  
1966  
1967  
1968  
1969  
1969  
1970  
1971  
1972  
1973  
1974  
1975  
1976  
1977  
1978  
1979  
1979  
1980  
1981  
1982  
1983  
1984  
1985  
1986  
1987  
1988  
1989  
1989  
1990  
1991  
1992  
1993  
1994  
1995  
1996  
1997  
1998  
1999  
1999  
2000  
2001  
2002  
2003  
2004  
2005  
2006  
2007  
2008  
2009  
2009  
2010  
2011  
2012  
2013  
2014  
2015  
2016  
2017  
2018  
2019  
2019  
2020  
2021  
2022  
2023  
2024  
2025  
2026  
2027  
2028  
2029  
2029  
2030  
2031  
2032  
2033  
2034  
2035  
2036  
2037  
2038  
2039  
2039  
2040  
2041  
2042  
2043  
2044  
2045  
2046  
2047  
2048  
2049  
2049  
2050  
2051  
2052  
2053  
2054  
2055  
2056  
2057  
2058  
2059  
2059  
2060  
2061  
2062  
2063  
2064  
2065  
2066  
2067  
2068  
2069  
2069  
2070  
2071  
2072  
2073  
2074  
2075  
2076  
2077  
2078  
2079  
2079  
2080  
2081  
2082  
2083  
2084  
2085  
2086  
2087  
2088  
2089  
2089  
2090  
2091  
2092  
2093  
2094  
2095  
2096  
2097  
2098  
2099  
2099  
2100  
2101  
2102  
2103  
2104  
2105  
2106  
2107  
2108  
2109  
2109  
2110  
2111  
2112  
2113  
2114  
2115  
2116  
2117  
2118  
2119  
2119  
2120  
2121  
2122  
2123  
2124  
2125  
2126  
2127  
2128  
2129  
2129  
2130  
2131  
2132  
2133  
2134  
2135  
2136  
2137  
2138  
2139  
2139  
2140  
2141  
2142  
2143  
2144  
2145  
2146  
2147  
2148  
2149  
2149  
2150  
2151  
2152  
2153  
2154  
2155  
2156  
2157  
2158  
2159  
2159  
2160  
2161  
2162  
2163  
2164  
2165  
2166  
2167  
2168  
2169  
2169  
2170  
2171  
2172  
2173  
2174  
2175  
2176  
2177  
2178  
2179  
2179  
2180  
2181  
2182  
2183  
2184  
2185  
2186  
2187  
2188  
2189  
2189  
2190  
2191  
2192  
2193  
2194  
2195  
2196  
2197  
2198  
2199  
2199  
2200  
2201  
2202  
2203  
2204  
2205

175 In such a fluvial deposit  
176 respect to the specific charac-  
177 the number of depositional  
178 degree of transportation of the  
179 allochthonous assemblage).

### **180 3. Material and methods**

### **181 3.1. Data collection and sub**

The present spatial taphonomic analysis focused on stratified specimens ( $n = 79$ ) from Geo 2a, whose spatial coordinates were available for all specimens. The area of analysis covers the period from 2015 until 2017. The sample included mostly macromammal remains ( $n = 707$ , 89%), undetermined isolated bone fragments ( $n = 70$ ), birds ( $n = 12$ ) and turtle ( $n = 8$ ) remains. A sub-sample ( $n = 249$ ) was further subset for the fabric analysis described below. Stratified specimens from Geo 2a collected during the test excavation of 2014, or subsequently found in plaster-jackets with concentration of bones during the lab preparation were excluded due to the lack of precise spatial coordinates. The very small sample ( $n = 4$ ) of micromammal remains was also not included in the spatial and faunal analyses. Faunal analysis was



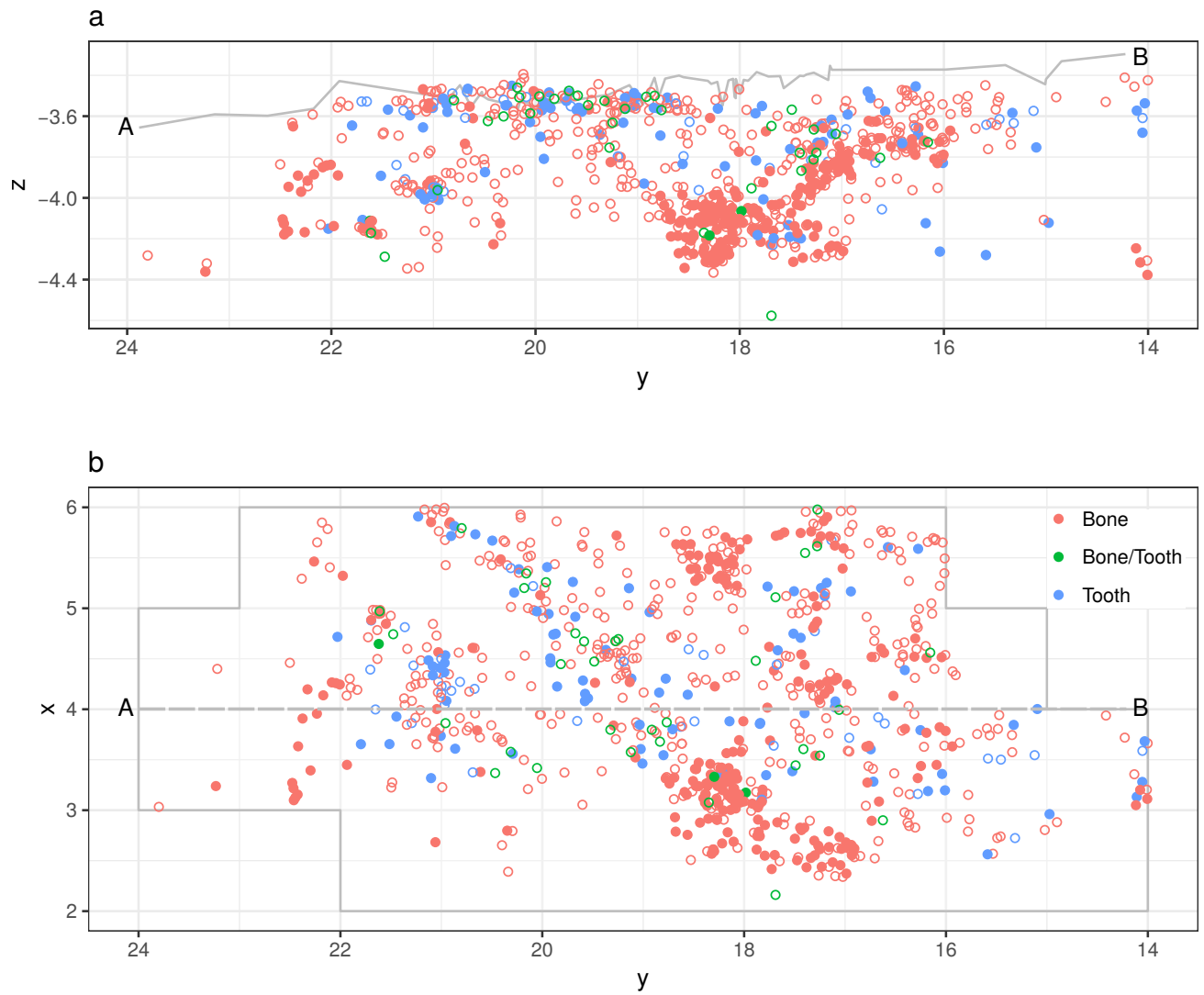


Figure 4: Vertical (a) and horizontal (b) distribution of the sampled fossil specimens from Tsiotra Vryssi (excavations 2015-2017). Filled circles mark complete specimens, hollow circles mark fragmented ones. Grey continuous line in a) marks the Geo 1/2 erosional contact, as recorded at the AB transect marked in b).

conducted on a sub-sample of complete or fragmented, isolated<sup>269</sup> or articulated macromammal remains (n = 707). Further sub-<sup>270</sup> setting strategies are described below.<sup>271</sup>

As for the AMS analysis, we collected 18 cylindrical ori-<sup>272</sup> ented samples ( $\varnothing = 2.5$  cm) from the middle part of the fossil-<sup>273</sup> iferous unit Geo 2a (Fig. 3). AMS analysis was performed at<sup>274</sup> the Alpine Laboratory of Paleomagnetism in Peveragno (Italy)<sup>275</sup> using a AGICO KLY-3 Kappabridge susceptibility meter (15-<sup>276</sup> positions, manual oriented).<sup>277</sup>

In order to investigate the micromorphological properties<sup>278</sup> of the Geo 2a unit (i.e., sedimentary structures and pedogenetic<sup>279</sup> features), two blocks of undisturbed sediment were collected<sup>280</sup> from the excavation area; one (TVB-Z 1) from the middle part<sup>281</sup> of the unit and the other (TVB-Z 2) from the topmost 30 cm<sup>282</sup> of it (Fig. 3). The blocks were later consolidated for prepara-<sup>283</sup> tion of thin sections following the methods described in Murphy<sup>284</sup> (1986)).<sup>285</sup>

appendicular (n = 122), undetermined (n = 93), axial and cra-<sup>286</sup> nial (n = 12) fragments - and due to the low percentage (9%, n = 22) of complete bones - 17 limb bones, 4 scapulae and a rib.

We applied Rayleigh and omnibus tests of uniformity, such as Kuiper, Watson and Rao (Jammalamadaka et al., 2001), to test the isotropic orientation of the fossil specimens. Whereas the Rayleigh test assumes a unimodal distribution and assess the significance of the sample mean resultant length ( $\bar{R}$ ), the omnibus tests detect multimodal departures from the null hy-<sup>287</sup> pothesis of circular isotropy.

Rose and equal area Schmidt diagrams were used as ex-<sup>288</sup> ploratory data analysis tools to visualise the sample distribution. Compared to the widely used rose diagrams, which plot the cir-<sup>289</sup> cular distribution of the bearing values, the Schmidt equal area diagram informs about the distribution of the three-dimensional orientation (plunge and bearing) of the elements (Fiorillo, 1988). Points plotting at the margin of the globe indicate planar fabric, whereas points towards the centre have higher dip angles.<sup>290</sup>

The Woodcock diagram (Woodcock and Naylor, 1983), based on three ordered normalised eigenvalues ( $S_1, S_2, S_3$ ), was used to discriminate between linear (cluster), planar (girdle) and isotropic distributions. In the Woodcock diagram, the C parameter ( $C = \ln(S_1/S_3)$ ) expresses the strength of the preferential orientation, and its significance is evaluated against critical values from sim-<sup>291</sup> ulated random samples of different sizes. A perfect isotropic distribution would plot at the origin, with equal eigenvalues ( $S_1 = S_2 = S_3 = 1/3$ ). On the other hand, the K parameter ( $K = \frac{\ln(S_1/S_2)}{\ln(S_2/S_3)}$ ) expresses the shape of the distribution, and it ranges from zero (uni-axial girdles) to infinite (uni-axial clus-<sup>292</sup> ters).<sup>293</sup>

In a fluvio-lacustrine environment a cluster distribution would suggest a strong preferential orientation of the sample, such as in the case of channelised water flows (Petraglia and Potts, 1994), whereas a girdle distribution a weaker preferential orientation, spread over a wider range of directions. Overland flows have been interpreted to produce such a pattern (Organista et al., 2017). On the other hand, a isotropic distribution would suggest that post-depositional disturbance by water flows was not strong enough to preferentially orient the assemblage (Domínguez-Rodrigo et al., 2014a). However, a variety of taphonomic processes can produce similar patterns. Fabric analysis, although very informative, has low power by itself. In order to overcome the intrinsic limitations of the fabric analysis, a multivariate approach to site formation and modification processes should be employed (Lenoble and Bertran, 2004).

### 3.2.2. Geostatistics

Geostatistics refer to a body of concepts and methods typ-<sup>294</sup> ically applied to a limited sample of observations of a continuous variable, for example environmental variables. Geostatistics thus aim to estimate the variance and spatial correlation of known observations and predict, using interpolation meth-<sup>295</sup> ods such as Kriging, unknown values of the variable at non-<sup>296</sup> observed locations. Moreover, by using directional variograms, geostatistics enable the identification of spatial anisotropy (i.e., directional patterns). Since the vast majority of spatial statistics assume stationarity and isotropy, it is well understood that a

## 3.2. Spatial anisotropy

Different methods have been developed in neighbouring dis-<sup>288</sup> ciplines to detect spatial anisotropy. Here we use circular statis-<sup>289</sup> tics for the fabric analysis of taphonomic elements; geostatis-<sup>290</sup> tics (directional variograms), wavelet analysis and point pattern<sup>291</sup> analysis for detecting anisotropy at the assemblage level.<sup>292</sup>

### 3.2.1. Fabric analysis

The first controlled experiments and analyses of the ori-<sup>295</sup> entation and dispersal of disarticulated mammal bones as indi-<sup>296</sup> cators of the depositional context, carried out by Toots (1965)<sup>297</sup> and Voorhies (1969), led to an increasing number of studies on<sup>298</sup> the effects of water flows on natural and anthropogenic faunal<sup>299</sup> assemblages (Aramendi et al., 2017; Benito-Calvo and de la<sup>300</sup> Torre, 2011; Cobo-Sánchez et al., 2014; de la Torre and Benito-<sup>301</sup> Calvo, 2013; Domínguez-Rodrigo et al., 2014a, 2012, 2014d;<sup>302</sup> Fiorillo, 1991; Nash and Petraglia, 1987; Organista et al., 2017;<sup>303</sup> Petraglia and Nash, 1987; Petraglia and Potts, 1994; Schick,<sup>304</sup> 1987, among others).<sup>305</sup>

Whereas most of these studies have been conducted on dis-<sup>306</sup> articulated long bones or elongated bone fragments - which<sup>307</sup> were observed to preferentially align their a-axes along the di-<sup>308</sup> rection of the flow - relatively few have investigated the hy-<sup>309</sup> draulic behaviour of articulated skeletal elements. Flume ex-<sup>310</sup> periments conducted by Coard and Dennell (1995) and Coard<sup>311</sup> (1999) demonstrated that articulated bones display a greater<sup>312</sup> transport potential than disarticulated ones when the articulated<sup>313</sup> elements align themselves. However, they also noted that skele-<sup>314</sup> tal parts with a higher number of articulated elements, such as<sup>315</sup> complete limbs, may show weak preferential orientation when<sup>316</sup> assuming disorganised spatial configuration, i.e., when not aligned.<sup>317</sup> Therefore, articulated bones, although relatively common at TSR<sup>318</sup> (Fig. 2a,b,c,d), were not included in the fabric analysis.<sup>319</sup>

In this study we applied circular statistics to a subset of 249<sup>319</sup> non-articulated, elongated bone specimens, having length >= 20mm<sup>320</sup> (Domínguez-Rodrigo et al., 2014d). No distinction of<sup>321</sup> skeletal elements was made, due to the high percentage (91%,<sup>322</sup> n = 227) of fragmented remains in the analysed sample - mostly<sup>323</sup>

misinterpretation of spatial anisotropy may result in inaccurate spatial modelling and prediction.

Although well known in ecological studies, only a relatively small number of studies have explicitly applied geostatistics to the study of site formation and modification processes, using directional variograms to investigate the specimens size spatial distributions (Domínguez-Rodrigo et al., 2014a,c), or to specifically detect spatial anisotropy of archaeological assemblages (Bevan and Conolly, 2009; Markofsky and Bevan, 2012).

In order to investigate spatial anisotropy in the distribution of the TSR fossil assemblage and identify spatial continuity in some directions more than others, we used directional variograms and variogram maps. The studied sample includes 797 recorded specimens (isolated or articulated, complete or fragmented bones and teeth) unearthed from Geo 2a and included in the 34 m<sup>2</sup> window of analysis (Fig. 4). The same sample was used for the wavelet and point pattern analyses.

Specifically, plotting the semi-variance between the variable values of sampled point pairs as a function of distance (spatial lag) between these pairs, directional variograms are used to model the spatial variation at multiple scales and different directions. Three parameters (*nugget*, *range* and *sill*) are estimated from an experimental variogram to fit a theoretical omnidirectional variogram. The *nugget* is used to account for spatial variability at very short distances. The *range* indicates the maximum distance up to which there is spatial correlation. At longer distances the semi-variance levels off forming the *sill*, indicating independence between pairs of sample separated by that minimum distance (Dale and Fortin, 2014; Lloyd and Atkinson, 2004). Thus, we plotted the experimental directional variogram against the theoretical omnidirectional variogram. A directional semi-variance lower than the fitted omnidirectional variogram indicates continuity in the analysed direction. We selected for our analysis the N-S (0°), E-W (90°), NE-SW (45°) and NW-SE (135°) geographical directions. In addition to the directional variograms, variogram maps are visual representations of the semi-variance: the anisotropy is represented by an ellipse, its axes being proportional to the variation expected in each direction. Thus, the direction of maximum anisotropy corresponds with the major axis of the ellipse (Legendre and Legendre, 2012).

### 3.2.3. Wavelet analysis

As a second method for the detection of spatial anisotropy at the assemblage level we used the wavelet analysis. Wavelet analysis, commonly applied in mathematics for signal processing, has relatively wide application in palaeoclimatology and palaeoecology, but is seldom used in studies on site formation processes (Markofsky and Bevan, 2012).

Unlike the geostatistics approach to the analysis of spatial anisotropy, which is based on a transformation of point values into a continuous surface, the wavelet approach does not apply any transformation, but identifies the elements (points) of a pattern merely by their location. In this regard, the wavelet analysis does not suffer from the arbitrary choice of a surface smooth parameter, as in the case of geostatistics.

For each specific point of the pattern, a wheel of 360 sectors of 1° is used to measure the average variance in the angles between point pairs (Rosenberg, 2004). The significance of the wavelet analysis is evaluated against 199 Monte Carlo simulations of the observed pattern under the null hypothesis of randomness. The variance is plotted as a function of angle measurements. Direction is measured anti-clockwise from East (i.e., 0° is East, 90° is North). When the distribution of the observed values (dashed line) wanders above the simulated values (continuous line), the pattern shows significant anisotropy in that direction.

### 3.2.4. Point pattern analysis

A spatial point pattern is the outcome of a random spatial point process. Any natural phenomenon which results in a spatial point pattern, such as a distribution pattern of fossils, can be viewed as a point process (Baddeley et al., 2015). Therefore, the analysis of a spatial point pattern ultimately addresses the nature of the point process that generated the pattern. Point pattern analysis has been specifically applied to the study of site formation and modification processes by a relatively small number of studies (Domínguez-Rodrigo et al., 2014a, 2017, 2014c; Giusti and Arzarello, 2016; Giusti et al., in press; Lenoble et al., 2008; Organista et al., 2017). However, this analytical method has never been used to detect anisotropy in the distribution patterns of archaeological or palaeontological assemblages. Nevertheless, detecting anisotropy is an essential part of any spatial analysis. Standard statistical tools in spatial point pattern analysis rely on crucial assumptions about the point process itself: a point process is assumed to be stationary and/or isotropic if its statistical properties are not affected by shifting and/or rotating the point process.

In order to further assess the presence of anisotropy in the distribution pattern of the TSR assemblage, we specifically applied the point pair distribution function ( $O_{r1,r2}(\Phi)$ ; Baddeley et al., 2015). The function estimates the probability distribution of the directions of vectors joining pairs of points that lie more than  $r1$  and less than  $r2$  units apart. With selected different distances  $r1$  and  $r2$ , the function estimates the multiscale variation of anisotropy. Results are visualised in rose diagrams, where the direction is measured counter-clockwise from East (0°).

At the supra-element assemblage level, spatial anisotropy is expected to be detected in a fluvial depositional environment, and most likely to share the same preferential orientation with taphonomic elements. Characteristic elongated lag deposits are typical patterns observed in association with water-flows dragging materials in one direction, the same as the main orientation of the elements (Domínguez-Rodrigo et al., 2012).

### 3.3. Anisotropy of magnetic susceptibility (AMS)

The anisotropy of magnetic susceptibility (AMS) is a technique used to identify preferred orientation of magnetic minerals in rocks and unconsolidated sediments (Hrouda, 1982; Tarling and Hrouda, 1993). It is based on the principle that, when a magnetic field is applied to a sample, the induced magnetisation depends on the bulk orientation of its magnetic constituents. In turn, the AMS magnitude depends on both the

435 anisotropy of individual magnetic particles and the degree of<sub>480</sub>  
 436 their alignment. Particle anisotropy can be related to either<sub>481</sub>  
 437 crystalline (anisotropy along a specific crystal plane or axis)<sub>482</sub>  
 438 or shape (anisotropy along the long axis of the particle) charac-<sub>483</sub>  
 439 teristics. Since in most magnetic minerals forming sedimentary<sub>484</sub>  
 440 particles the long crystallographic axis is the easiest to magne-<sub>485</sub>  
 441 tise (e.g., magnetite), the shape anisotropy is generally domi-<sub>486</sub>  
 442 nant, with few exceptions (e.g., haematite).<sub>487</sub>

443 The magnetic susceptibility is represented by three symmet-<sub>488</sub>  
 444 ric tensors describing an ellipsoid with three susceptibility axes<sub>489</sub>  
 445 named K1 to K3 and ordered by decreasing susceptibility. The<sub>490</sub>  
 446 orientation of the ellipsoid is evaluated projecting the ellipsoid<sub>491</sub>  
 447 axes on an equal-area projection stereogram. Thus, the shape of<sub>492</sub>  
 448 the ellipsoid is evaluated using the Flinn or Jelinek scatter plots.<sub>493</sub>  
 449 In a Flinn (F/L) diagram the foliation along the horizontal axis<sub>494</sub>  
 450 ( $F = K2/K3$ ; Stacey et al., 1960) is plotted against the lineation<sub>495</sub>  
 451 along the vertical axis ( $L = K1/K2$ ; Balsey and Buddington,<sub>496</sub>  
 452 1960). Values of  $F/L < 1$  indicate oblate ellipsoids (i.e., disc-<sub>497</sub>  
 453 shaped), whereas values of  $F/L > 1$  indicate prolate ellipsoids<sub>498</sub>  
 454 (i.e., cigar-shaped) with the axial ratios increasing with distance<sub>499</sub>  
 455 from the origin. Alternatively, the AMS magnitude and shape<sub>500</sub>  
 456 can be visualised on the Jelinek shape plot (Jelinek, 1981), by<sub>501</sub>  
 457 using the corrected anisotropy degree<sub>502</sub>

$$Pj = \exp \sqrt{2[(\ln K1 - k)^2 + (\ln K2 - k)^2 + (\ln K3 - k)^2]}$$

458 where

$$k = \frac{\ln K1 + \ln K2 + \ln K3}{3}$$

459 and the shape parameter

$$T = \frac{\ln L - \ln F}{\ln L + \ln F}$$

460 where samples are prolate for  $-1 < T < 0$  or oblate for  $0 <$   
 461  $T < 1$ .<sub>515</sub>

462 In sediments, oblate ellipsoids with imbrication angles less<sub>516</sub>  
 463 than  $20^\circ$  are considered diagnostic of primary depositional pro-<sub>517</sub>  
 464 cesses (Hamilton and Rees, 1970; Hrouda, 1982; Lanza and<sub>518</sub>  
 465 Meloni, 2006; Liu et al., 2001; Tarling and Hrouda, 1993). In<sub>519</sub>  
 466 turn, prolate ellipsoids mostly relate to post-depositional defor-<sub>520</sub>  
 467 mation (e.g., rocks recording tectonic or metamorphic strain),<sub>521</sub>  
 468 especially when the magnetic anisotropy is high (Hrouda and<sub>522</sub>  
 469 Janák, 1976).<sub>523</sub>

#### 470 3.4. Differential preservation

471 Differential preservation, or taphonomic survival, refers to<sub>527</sub>  
 472 the proportion of taphonomic elements being preserved after<sub>528</sub>  
 473 the action of environmental factors (Fernández-López, 2006).<sub>529</sub>  
 474 Selective preservation arises from the differential modification<sub>530</sub>  
 475 of taphonomic entities, by interaction of inherent properties of<sub>531</sub>  
 476 the entities with the external environmental factors. Skeletal<sub>532</sub>  
 477 elements representation is among the key variables potentially<sub>533</sub>  
 478 indicative of the selective action of water-flows (Behrensmeyer,<sub>534</sub>  
 479 1975b; Kaufmann et al., 2011; Voorhies, 1969, among others).<sub>535</sub>

Other variables, not considered in this preliminary study, include breakage patterns, disarticulation patterns and bone surface modifications.

The pioneering flume experiments by Voorhies (1969) on disarticulated, complete sheep and coyote bones resulted in a three-group classification of fluvial transport susceptibility of skeletal elements, subsequently elaborated by Behrensmeyer (1975b). Since shape and structural density have been found to influence the transportability of skeletal elements (Behrensmeyer, 1975b; Boaz, 1982), assemblages subject to moderate to high-energy water-flows typically show an under-represented number of smaller, less dense bones. The Voorhies Group I (rib, vertebra, sacrum, sternum) is the most easily affected by fluvial transport; thus its presence or absence in the fossil assemblage informs about the degree of disturbance by water-flows. In turn, the proportion between the represented Voorhies Groups provides evidence for the degree of preservation of the assemblage (Behrensmeyer, 1975b). We included in the Voorhies groups only complete, non-articulated macromammal bones (plus rami of mandibles, and maxillae) of adult individuals - the very few specimens of juvenile individuals, having different hydraulic behaviour, were excluded. Our grouping criteria followed the classification reported in Lyman (1994, Tab.6.5). Carpals, tarsals and sesamoids were included in Voorhies Group I/II, as the phalanges; maxillae in Group II/III, as the mandibular rami. The studied sample included 147 specimens of Perissodactyla (n = 59), Artiodactyla (n = 41), Carnivora (n = 12) and indeterminate taxa (n = 35). The distribution of determinate Voorhies Groups was further categorised in 5 size classes, following the body mass (BM) classification of Palombo (2010, 2016), modified for *Ursus etruscus* after Koufos et al. (in press). The first group (BM1), not present so far in our collection, includes mammals weighing less than 10 kg; BM2 ranges from 10 to 59 kg (*Canis etruscus*); BM3 from 60 to 249 kg (*Ursus etruscus*, medium-sized Cervidae); BM4 from 250 to 1000 kg (*Equus*, *Bison*, *Praemegaceros*). We excluded from the Voorhies Groups specimens attributed to BM5, that includes very large mammals over 1000 kg weight (Rhinocerotidae and Elephantidae). Nevertheless, their skeletal element representation was analysed following the Fluvial Transport Index (FTI) classification of Frison and Todd (1986). Undetermined taxa or BM classes - yet in the BM2-BM4 range - were also included in the analysis (named NA in Fig. 10).

Closely related to the Voorhies Groups, the ratio of complete isolated teeth/vertebrae (T/V) is another indicator of the depositional environment (Behrensmeyer, 1975b). High-energy fluvial deposits, such as channel-fills and -lag deposits, tend to have high T/V ratio, whereas a low T/V ratio characterises low-energy fluvial deposits, such as that of floodplain deltaic and lacustrine settings (Lyman, 1994).

Complementary to the hydraulic behaviour of complete, isolated faunal remains classified in the Voorhies Groups, the skeletal part representation of fragmented bones provides another indication of the assemblages degree of preservation (Domínguez-Rodrigo et al., 2017, 2014d; Pante and Blumenschine, 2010). Vertebrae and ribs, being mostly cancellous, fragile and comparatively less dense, are more susceptible to fragmentation and

537 transportation, even in low-energy conditions, with respect to  
 538 cranial and appendicular elements, which are more dense and  
 539 likely to survive in lag assemblages (Domínguez-Rodrigo et al.,  
 540 2017). In order to integrate the Voorhies Groups, we analysed  
 541 a sub-sample of 400 isolated macromammal specimens, com-  
 542 posed of 315 bone and tooth fragments, 78 complete teeth, 1  
 543 antler, and 6 appendicular bones of juvenile or BM5 specimens.

544 Finally, the distribution of articulated bones was analysed  
 545 by anatomical regions. A sub-sample of 50 articulated macro-  
 546 mammal units of 154 bone elements were classified as axial  
 547 (vertebrae, ribs) or appendicular (humeri, femura, radii, tibiae,  
 548 metapodials, carpals/tarsals and phalanges) units.

### 549 3.5. Reproducible research

550 The subset of the raw data collected for this study, neces-  
 551 sary to reproduce the reported results, is licensed, except where  
 552 otherwise specified, under the CC-BY-NC-ND-4.0 license and  
 553 publicly available at the DOI: [10.5281/zenodo.1435836](https://doi.org/10.5281/zenodo.1435836). The  
 554 repository includes in addition the code used to process and  
 555 reduce the data-set. The analyses were performed in R: a lan-  
 556 guage and environment for statistical computing (R Core Team,  
 557 2017); except for the wavelet analysis, performed using the  
 558 PASSaGE software, version 2 (Rosenberg and Anderson, 2011).  
 559 The commented R code needed to reproduce the reported anal-  
 560 yses is released under the MIT license in the same repository.  
 561 We provide as well a detailed description of the procedure used  
 562 in PASSaGE.

## 563 4. Results

### 564 4.1. Anisotropy of basic taphonomic elements

565 Circular statistics were applied for the fabric analysis of  
 566 basic taphonomic elements, i.e., isolated, not articulated elon-  
 567 gated complete bone specimens or bone fragments. Tab. 1 sum-  
 568 marises the results of the circular uniformity tests. The Rayleigh  
 569 test, which assumes a unimodal distribution, confirmed ( $p -$   
 570  $value = 0.001$ ) the significance of the sample mean resultant  
 571 length ( $\bar{R} = 0.165$ ). The value of  $\bar{R}$  close to 0 indicates that the  
 572 data are evenly spread around the mean direction ( $\bar{\theta} = 148^\circ$ , SE),  
 573 with relatively high standard deviation ( $\hat{\sigma} = 1.89$ ) and angular  
 574 variance ( $V = 48$ ). On the other hand, the Schmidt and rose  
 575 diagrams (Fig. 5a) showed a multimodal distribution, mostly  
 576 concentrated in the SE quadrant and with secondary peaks to  
 577 the N and SW. Accordingly, the Kuiper, Watson and Rao om-  
 578 nibus tests, all rejected the null hypothesis of uniformity at the  
 579 99% confidence level, thus suggesting a significant anisotropic  
 580 multimodal distribution of the fossil sample. Moreover, the  
 581 Schmidt diagram (Fig. 5a) showed a planar fabric of the sample  
 582 distribution, with points plotting predominantly on the edge of  
 583 the equal area hemisphere, thus indicating 0-to-low degree of  
 584 dip (mean plunge=12°; variance=1.5°).

585 In the Woodcock diagram (Fig. 5b), the  $C$  value (1.89) is  
 586 higher than the critical S1/S3 test value (1.44) for  $N=300$  at  
 587 99% confidence level. Thus, the data sample significantly  
 588 rejects the hypothesis of randomness in favour of a strong organ-  
 589 ised sample. The  $K$  value (0.11) plots the data sample close to  
 590  $K = 0$ , indicating uniaxial girdles (planar fabric).

Table 1: Values and  $p - values$  of circular uniformity test statistics.

Sample $n$	mean dir.	Rayleigh		Kuiper	
		$\bar{R}$	$p$	$V_n$	$p$
249	148°	0.165	0.001	2.3791	<0.

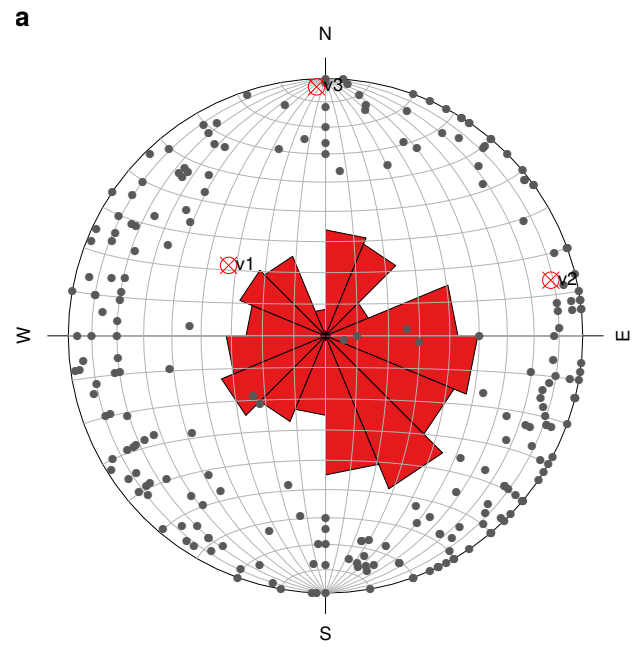


Figure 5: Rose and equal area Schimdt diagrams (a). Woodcock diagram (b).

591 4.2. Anisotropy of the taphonomic population

592 Geostatistics (directional variograms and variogram map),  
 593 wavelet and point pattern analyses were used for detecting anisotropy  
 594 at the assemblage level. Fig. 6a shows the kernel smooth den-  
 595 sity estimation ( $\sigma = 0.17$ ) of the sample distribution in the  
 596 study area. A preliminary visual examination suggests a NW-  
 597 SE oriented clustering of the assemblage, although interfered  
 598 with secondary NE-SW oriented dispersion. Fig. 6b shows the  
 599 variograms in the four main geographical directions (N-S, E-  
 600 W, NE-SW, NW-SE), plotted against the omnidirectional fitted  
 601 variogram. As a rule of thumb, in order to determine the spatial  
 602 structure of the sampled data, only the first two-thirds of the  
 603 variogram are interpreted (Dale and Fortin, 2014). The omni-  
 604 directional variogram (red line) indicates that at short distance  
 605 lags, the semi-variances are close to zero, indicating very strong  
 606 spatial structure (correlation). With longest distance lags, the  
 607 semi-variance rise to a plateau (*sill*) of lack of spatial corre-  
 608 lation. The semi-variance of the NW-SE (135°) direction is lower  
 609 than in the omnidirectional variogram, starting well before the  
 610 *sill*, thus indicating continuity (spatial correlation) in that di-  
 611 rection. Minor directional trends are also detected in the N-S  
 612 (0°), and to a lesser extent in the NE-SW (45°) directions. This  
 613 result is clearly confirmed by the diagonal striping in the vari-  
 614 ogram map (Fig. 6c). The map shows a major ellipse oriented  
 615 NW-SE, with minor parallel structures.

616 As for the wavelet analysis, Fig. 7 plots the variance as  
 617 function of the direction, ranging anti-clockwise from 0° (E)  
 618 to 180° (W). A major peak is evident at 135° (NW), wandering  
 619 way above the expected values for a random (isotropic) pattern.  
 620 A secondary significant peaks, although of much less intensity,  
 621 is present at 85° (N). In accordance with the directional vari-  
 622 ograms, the wavelet analysis indicates a significant anisotropy  
 623 in the NW-SE direction. Moreover, it suggests minor occur-  
 624 rence of points (specimens) in the N-S direction, as also indi-  
 625 cated by the geostatistics analysis. However, in contrast with  
 626 the directional variograms, the angular wavelet graph does not  
 627 support significant preferential orientation in the NE range (an-  
 628 gles between 0° and 90°).

629 Fig. 8 shows the results of our point pattern analysis and  
 630 specifically the point pair distribution function  $O_{r1,r2}(\Phi)$  for a  
 631 range of distances  $r_1 = 0.01$  m and  $0.25 < r_2 < 1.5$  m.  
 632 The plot illustrates the multiscale variation of anisotropy, from  
 633 a uniform, isotropic pattern (for  $r_2 = 0.25$  m), to increased  
 634 anisotropy in the NW-SE direction. The maximum anisotropy  
 635 is observed for  $r_2 = 1$  m, as elements at a maximum distance  
 636 of 1 m show the strongest directional pattern. With increased  
 637 distances of  $r_2 > 1$  m, the rose diagrams suggest the addition  
 638 of a second orthogonal NE-SW directional trend, which reflects  
 639 the parallel alternation of NW-SE bands in the assemblage dis-  
 640 tribution.

641 4.3. Anisotropy of magnetic susceptibility

642 In Fig. 9a, the AMS of the whole sample set ( $n = 18$ ) is in-  
 643 vestigated. The equal-area projection of the three susceptibility  
 644 axes K1-K3 (left-hand side of Fig. 9a) indicates high variabil-  
 645 ity of the axes orientation, with confidence angles of the K1

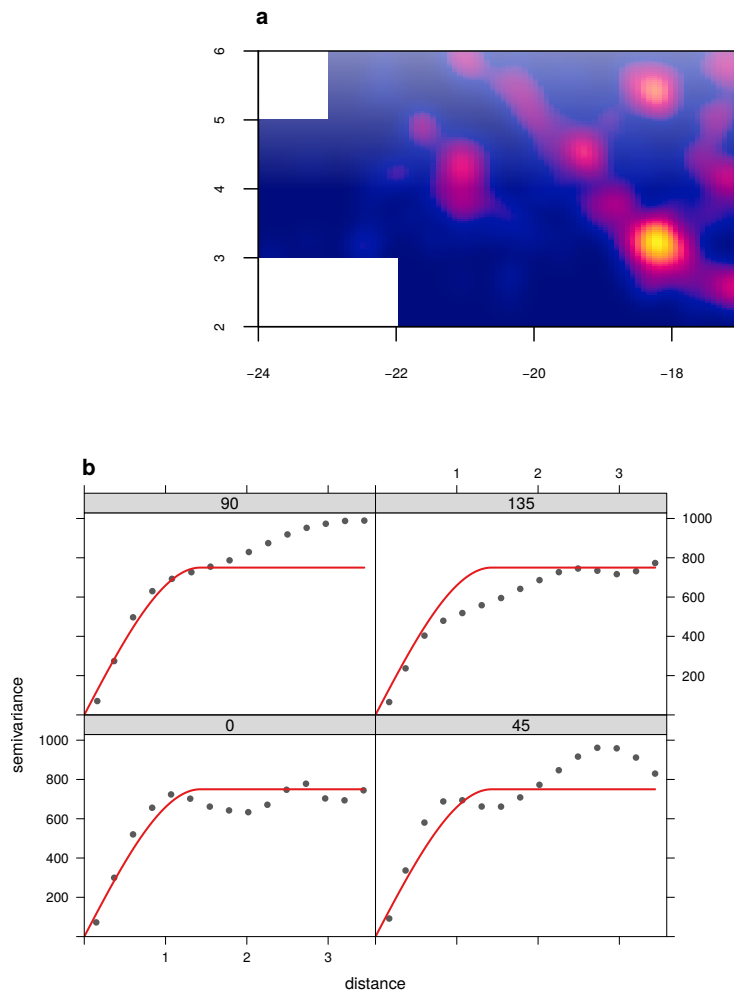


Figure 6: Kernel smoothed intensity function of the fossil assemblage (a). Directional variograms (4 clockwise directions from N-S, 0°) shown as grey points alongside the fitted omnidirectional variogram shown as a continuous red line (b) and variogram map (c).

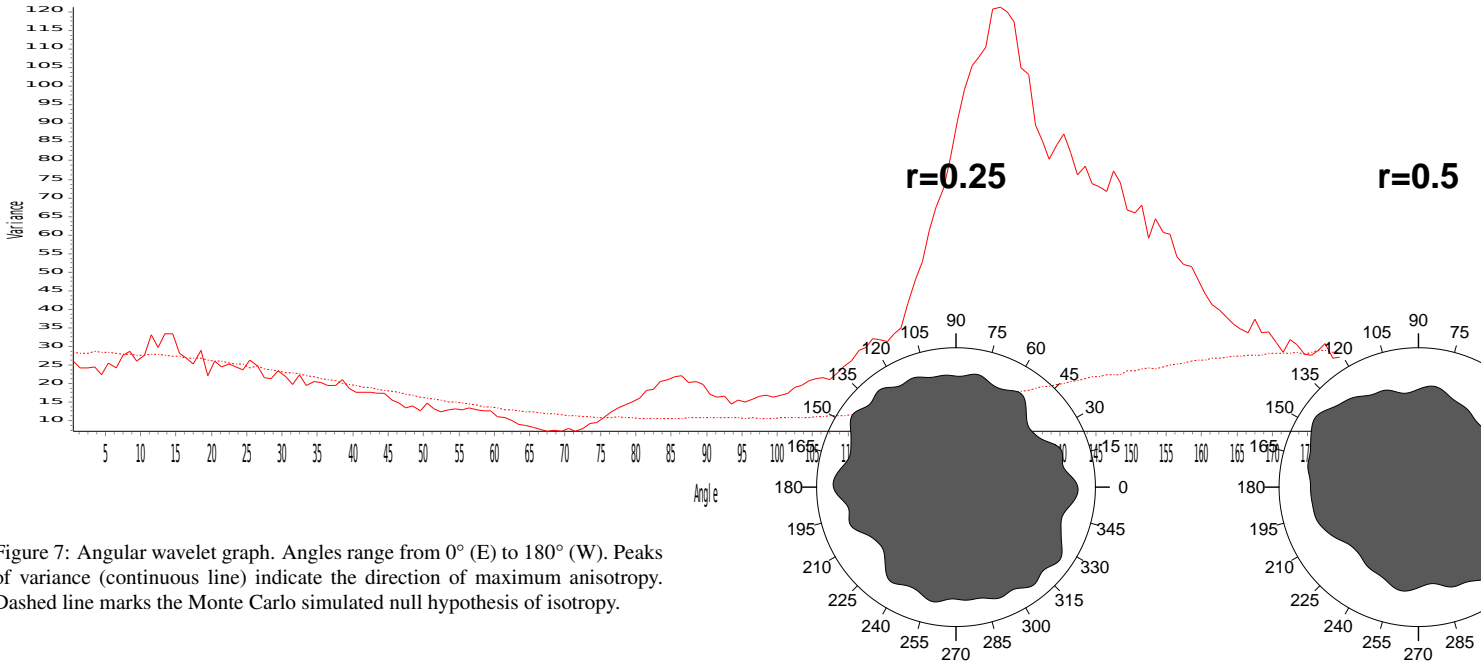


Figure 7: Angular wavelet graph. Angles range from  $0^\circ$  (E) to  $180^\circ$  (W). Peaks of variance (continuous line) indicate the direction of maximum anisotropy. Dashed line marks the Monte Carlo simulated null hypothesis of isotropy.

and K2 mean directions largely overlapping. This result suggests no preferential orientation of the axes. However, the Flinn and Jelinek plots (right-hand side of Fig. 9a) reveal the presence of 7 samples with prolate ellipsoids, thus suggesting the action of post-depositional deformation processes which could have obliterated the primary depositional pattern. Therefore, in order to overcome possible post-depositional noise, further AMS analysis focused only on a sub-set of samples showing oblate ellipsoids ( $n = 11$ ). In Fig. 9b, the equal-area projection shows a well defined clustering of the axes, with the maximum anisotropy axis K1 aligned along the NW-SE direction and the K3 imbrication angles varying within a wide range of angles (from  $4^\circ$  to  $85^\circ$ ). Because high K3 imbrication angles may result from post-depositional rehash of sediments, further analysis were conducted on a selection of 5 samples with K3 imbrication angles less than  $20^\circ$  (Hamilton and Rees, 1970; Hrouda, 1982; Lanza and Meloni, 2006; Liu et al., 2001; Tarling and Hrouda, 1993). In Fig. 9c, the equal-area projection indicates again a NW-SE orientation of the maximum anisotropy axis K1. Despite the small sample size, the AMS analysis suggests a weak anisotropy of magnetic sedimentary grains along a NW-SE direction.

#### 4.4. Differential preservation

Fig. 10a shows the distribution at the family level of the whole sampled material. Determined taxa included Perissodactyla, Artiodactyla, Carnivora and Proboscidea, together with a number of undetermined bone fragments (44%). The histogram shows the prominent presence of Equidae over other taxa (27%), followed by Bovidae (11%) and Cervidae (5%). However, it is worth noting the presence of very large mammals (body mass class BM5), such as Elephantidae and the rhinocerotid *Stephanorhinus* sp., and to a less extent, of carnivores, such as *Canis etruscus* and *Ursus etruscus*.

The distribution of the Voorhies Groups plotted by body

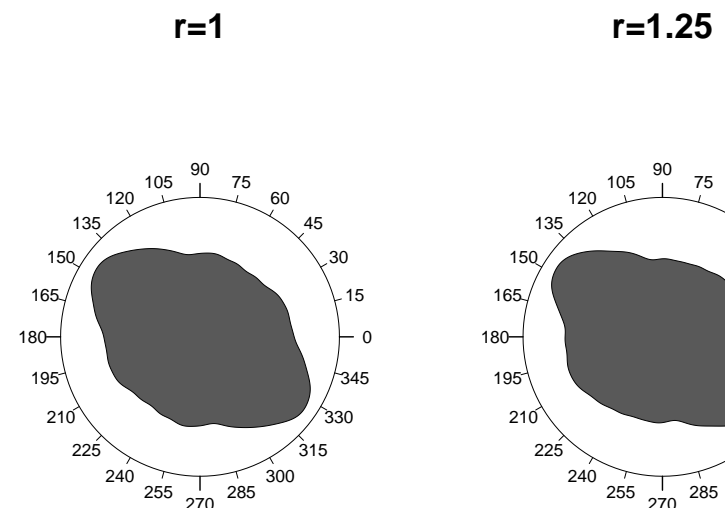


Figure 8: Rose diagrams of the point pair distribution function for a range of distances ( $0.25 < r_2 < 1.5\text{m}$ ). Direction is measured counter-clockwise from East ( $0^\circ$ ).

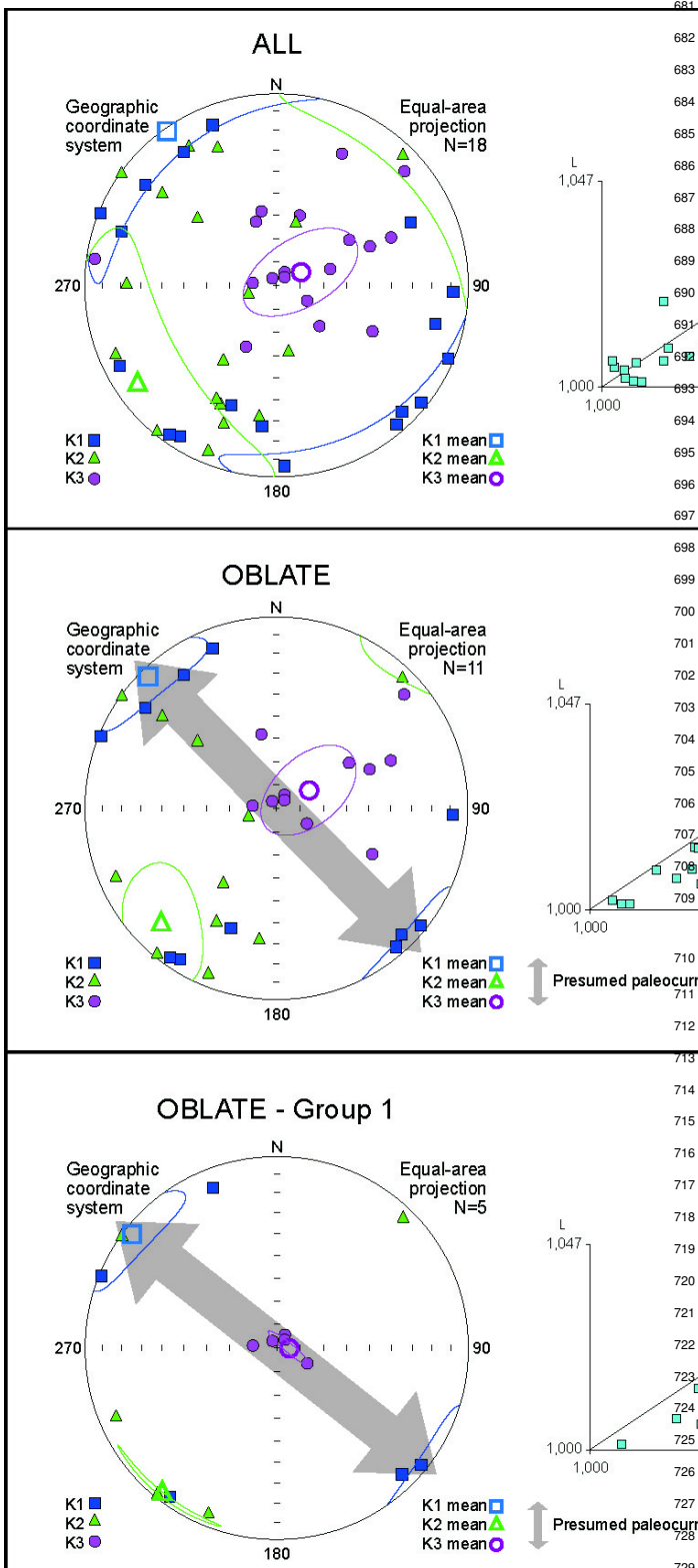


Figure 9: Equal-area projection stereogram (left-hand side) of the anisotropy axes K1, K2 and K3 (with  $K_1 > K_2 > K_3$ ) and Flinn and Jelinek plots (right-hand side) for a) all the samples; b) samples with oblate-shaped anisotropy ellipsoid; c) samples with  $K_3$  imbrication angle less than  $20-25^\circ$ .

mass classes is shown in Fig. 10b. BM1 is so far not present in the TSR assemblage, while BM2 includes the *C. etruscus*

BM3 includes the medium-sized Cervidae and *Ursus etruscus*, BM4 the medium- and large-sized *Equus* sp., *Bison* sp. and the large-sized cervid *Praemegaceros* sp. Notably, the Voorhies Group III is represented in Fig. 10b only by the crania of the carnivores *Canis* and *Ursus*. Moreover, the fossil record of *U. etruscus* included maxilla fragments (Voorhies Group II/III), isolated teeth, 2 articulated vertebrae and an ulna fragment. Specimens from the BM4 grouped mostly in H/II, II, I/II and showed lack of Voorhies Group I and III. On the other hand, the bulk of undetermined BM specimens plotted in Voorhies Group I/II, with some occurrence in Group I, II, and to a less extent in Group II/III.

Fig. 10c shows the side-by-side distribution of complete and fragmented isolated macromammal skeletal elements. Firstly, the skeletal element distribution of complete specimens suggests a very high teeth/vertebra ratio (7.8). The ratio (3) is

lower, but still relatively high when considering isolated, fragmented specimens. Limb bone and undetermined fragments represent the majority of the fragmented, isolated specimens, as compared to axial skeletal parts.

Accordingly, the prominent presence of appendicular skeletal elements over axial is also shown in the distribution of articulated specimens (Fig. 10d), which account for 22% of the sampled assemblage. Articulated lower limb elements (metapodials, carpals/tarsals, phalanges) represent the majority of bones, often articulated to fragmented upper elements (radii, tibiae, humeri, femora). Interestingly, some of the latter elements present carnivore gnawing marks (Fig. 2e).

#### 4.5. Micromorphology

The TVB-Z 1 block (Fig. 3) consists mostly of poorly sorted sandy silts, compositionally dominated by metamorphic quartz and accessory metamorphic minerals. From bottom to top, several sharp grain size breaks occur, which partition the sampled interval into mm-thick normally graded laminae, displaying an upward increase of matrix content (Fig. 11a). This includes clay infilling pore spaces (Fig. 11a) and suggests either flow velocity fluctuations or multiple waning depositional events. Birefringent illuvial clay coatings are also present along some voids (Fig. 11b), thus indicating incipient pedogenesis, likely due to temporary subaerial exposure (Kühn et al., 2010).

Most of the thickness of the TVB-Z 2 block (Fig. 3) displays similar characteristics to the TVB-Z 1 block, except for the presence of rolled soil clasts (pedorelicts; Fig. 11c), likely eroded from nearby locations (Cremaschi et al., In press). Conversely, the uppermost part of the sample (Fig. 11d) displays moderate clay illuviation along voids, sparse voids most likely related to bioturbation and impregnating redoximorphic features (Lindbo et al., 2010). The latter include Fe oxide hypocoatings on the groundmass, Fe/Mn oxide nodules with regular outline developed on quartz grains, and fragmented clay coatings.

Altogether, these features suggest that, after deposition, Geo 2a underwent moderate pedogenesis due to a relatively prolonged phase of subaerial exposure in a warm and possibly humid climate or while still saturated with water.

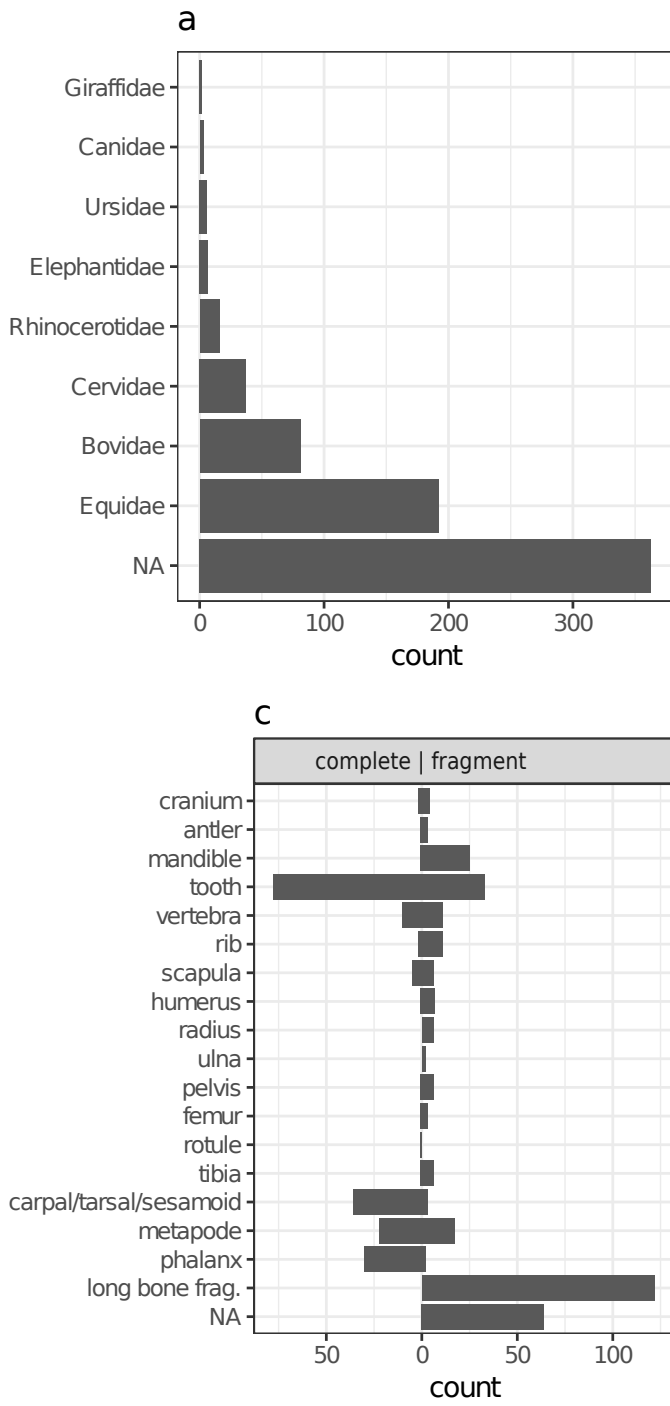
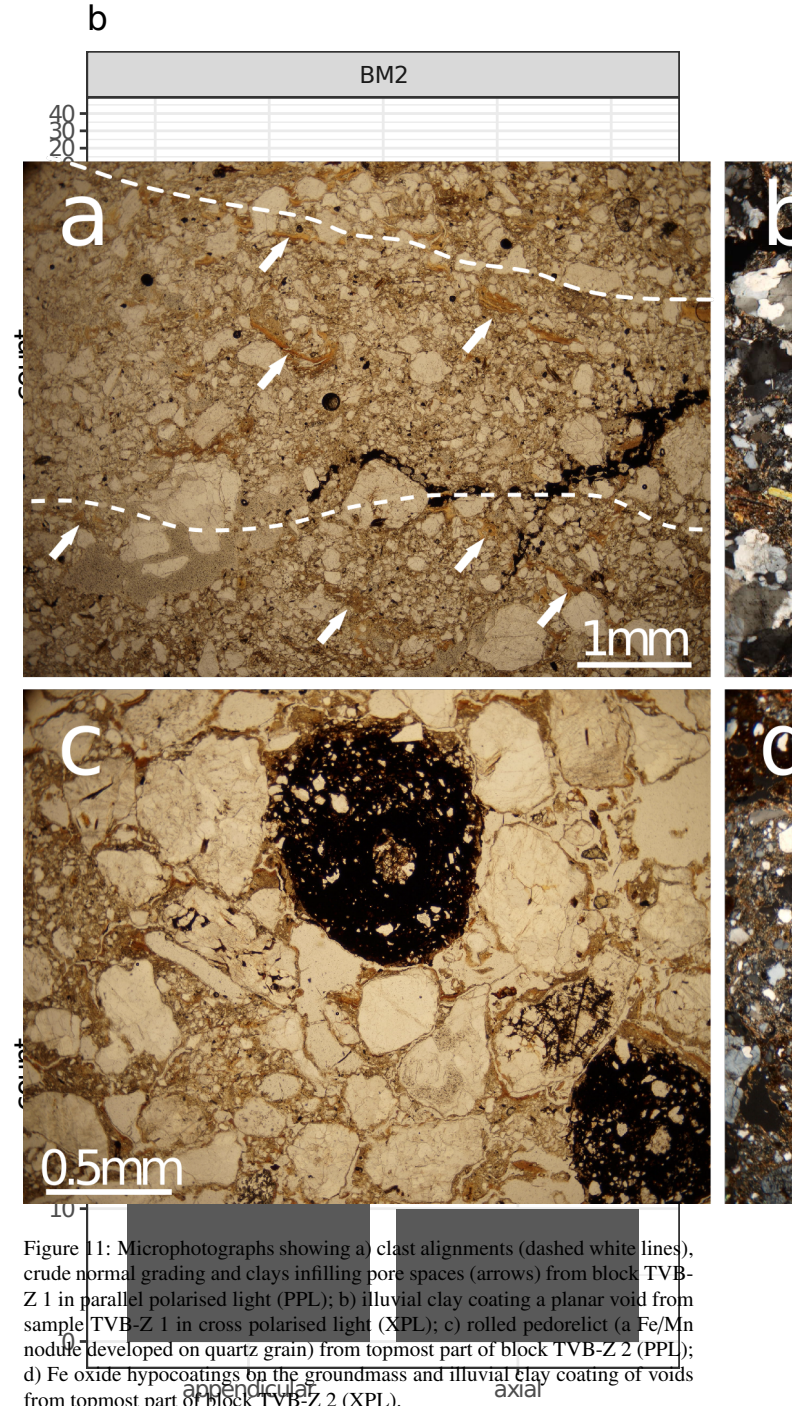


Figure 10: Distribution at the family level of the whole sampled material (a). Voorhies Groups distribution of the complete, isolated macromammal bones (plus rami of mandibles and maxillae) by body mass (BM) (b). Side-by-side distribution of complete/fragmented isolated macromammal skeletal elements (c). Skeletal region distribution of articulated macromammal specimens (d).



## 5. Discussion

1969, among others). However, spatial anisotropy at supra-element level of taphons or assemblages is an often neglected taphonomic criterion that should be reconsidered, especially in spatial taphonomic analyses of fluvial dispersion and accumulation processes. Nevertheless, standard spatial statistics rely on crucial assumptions about the isotropy of the spatial processes responsible for the observed spatial pattern (Baddeley et al., 2015).

We investigated the multilevel spatial anisotropy and selective composition of the fossiliferous deposit of Tsiotra Vryssi, from the fluvial Gerakarou Formation of the Mygdonia Basin, Greece. Specific research questions regarded the character and number of depositional processes and the degree of re-elaboration of the fossil record. Specific aspects of our results are discussed below.

### 5.1. Recursive anisotropy

Recursive anisotropy emerged at the level of basic taphonomic elements and at the assemblage level. Fabric analysis, geostatistics, wavelet and point pattern analyses all pointed to a preferential NW-SE orientation of the assemblage and the sub-sample of elongated bone specimens.

Fabric analysis, or the analysis of the orientation (plunge and bearing) of elongated elements, can provide valuable insight into taphonomic processes, allowing discrimination between different orientation patterns (isotropic, linear or planar). We analysed a sub-sample of not articulated, clearly elongated bone specimens, mostly limb bone fragments. Articulated units were excluded from the fabric analysis since experimental studies by Coard and Dennell (1995) and Coard (1999) reported that articulated units with a higher number of elements, such as complete limbs, may show weak preferential orientation when not aligned, as they often occur at TSR (Fig. 2c,d,e). Otherwise, the authors concluded that articulated bones showed a greater than expected hydraulic transport potential. Thus, their conspicuous presence in the TSR fossil record (about 22%) would not necessarily suggest an autochthonous deposit.

The results of the circular uniformity test statistics (Tab. 1) agreed upon rejecting the null hypothesis of uniformity, suggesting a significant anisotropic distribution of the fossil sample. The Schimdt and Woodcock diagrams in Fig. 5 indicated planar fabric (0-to-low degree of dip) and a girdle pattern, with preferential orientation towards the SE. In girdle distribution elements orient over a wider sector of angles than cluster distributions, yet showing higher anisotropy than random distributions. Whereas cluster, linear patterns are associated with channelised water-flows (Petruglia and Potts, 1994), girdle, planar patterns have been interpreted as products of overland flows (runoff; Organista et al., 2017). The preferential orientation of the sampled elongated bones suggests that the TSR fossil deposit most likely underwent relatively high-energy, but non-channelised NW-SE water-flows. However, anisotropy does not itself discriminate between allochthonous and autochthonous deposits. Autochthonous lag assemblages undergoing minimal re-sedimentation could also exhibit significant anisotropic spatial patterns (Domínguez-Rodrigo et al., 2012, 2014b, 2017, 2014c). Since a wide range of different taphonomic processes

Spatial taphonomy has recently emerged as a new methodological framework complement to the traditional taphonomic approach (Domínguez-Rodrigo et al., 2017). By using spatial statistical methods, spatial taphonomy aims to investigate the multiscale and multilevel spatial properties of different taphonomic entities (*sensu* Fernández-López, 2006). Indeed, taphonomic alteration processes work simultaneously, at different scales, on entities of different level of organisation, from the basic taphonomic elements (bone specimens), to higher level taphonomic groups (taphons) or populations (assemblages). For example, dispersion processes of taphonomic elements may modify their spatial location, orientation and removal degree. At the same time, dispersion of taphonomic elements may also cause changes in the density, spatial distribution and representatives of elements of each taphon or taphonic population (Fernández-López, 2006). Thus, beside the traditional taphonomic approach, the results of spatial taphonomy are of great importance for investigating the natural or cultural processes of dispersal and accumulation of faunal or cultural remains, in turn with consequences for palaeoecological reconstructions, biochronological estimates and past human behavioural inferences.

In this regard, this study offers an initial contribution to the development of a so far non-existent referential framework for the spatial taphonomic interpretation of palaeontological or archaeological assemblages (Domínguez-Rodrigo et al., 2017). Indeed, the taphonomic study of non-human related bone assemblages has great importance for archaeological research as well. As an example, water-flow processes are recognised to be among the most important natural processes in the formation and modification of a significant percentage of the vertebrate fossil and archaeological sites alike (Behrensmeyer, 1975a, 1982, 1988; Coard, 1999; Coard and Dennell, 1995; Petruglia and Nash, 1987; Petruglia and Potts, 1994; Schiffer, 1987; Voorhies, 1969, among others). Under the effect of water-flows, assemblages may adopt a variety of forms, ranging from (peri)autochthonous rearranged assemblages and biased lag assemblages to transported, allochthonous assemblages (Behrensmeyer, 1988; Domínguez-Rodrigo and García-Pérez, 2013). One fundamental assumption behind reliable inferences on past human behaviour is the pristine preservation of the depositional context. Therefore, it is essential, in order to fully comprehend the archaeological record, to test within a referential framework alternative taphonomic hypotheses.

In this study, taphonomic dispersion and accumulation processes were analysed focusing on a specific aspect - anisotropy - of the spatial properties of taphonomic entities. A multilevel analysis of anisotropy was conducted at the level of basic taphonomic elements and at the assemblage level. Anisotropy, defined as the preferential orientation of skeletal elements, constitutes a fundamental part of any taphonomic study (Aramendi et al., 2017; Benito-Calvo and de la Torre, 2011; Cobo-Sánchez et al., 2014; de la Torre and Benito-Calvo, 2013; Domínguez-Rodrigo et al., 2014a, 2012, 2014d; Fiorillo, 1991; Nash and Petruglia, 1987; Organista et al., 2017; Petruglia and Nash, 1987; Petruglia and Potts, 1994; Schick, 1987; Toots, 1965; Voorhies,

can produce similar patterns, an unequivocal discrimination based only on fabric observations is seldom possible, and other taphonomic criteria should be considered (Lenoble and Bertran, 2004).

Geostatistics, wavelet and point pattern analyses were applied in order to detect anisotropy of the TSR fossil assemblage. All these different methods agreed on identifying a preferentially NW-SE oriented distribution. Four directional variograms and a variogram map (Fig. 6b,c) were calculated from a kernel density estimation of the assemblage spatial distribution (Fig. 6a). Small, dense clusters of fossils, although occurring at different elevations in the 1m-thick vertical distribution (Fig. 4a), concatenate along a prevailing NW-SE direction. Secondary minor directions (N-S and NE-SW) were identified in the directional variograms (Fig. 6b). In the same manner, the wavelet graph (Fig. 7) and the rose diagrams (Fig. 8) also detected a strong preferential NW-SE directional distribution. Similar elongated lag deposits are typically associated with water-flows dragging material in one direction (Domínguez-Rodrigo et al., 2012).

These observations are in agreement with the AMS results. Despite the small sample size, the AMS results suggest relatively strong anisotropy, with a mean K1 axis oriented NW-SE and a mean K2 axis oriented NE-SW, although with much smaller confidence angles (Fig. 9). Since K1 (i.e., the axis of maximum anisotropy) should reflect the bulk orientation of the elongated axis of the ferro/paramagnetic sedimentary particles, it might be concluded that AMS hints at a NW-SE oriented anisotropy.

Thus, the observed recursive multilevel anisotropy patterns most probably points to the action of NW-SE oriented water flows, at the specific location of the TSR site. However, both analyses of isotropy at element level (fabric analysis) and assemblage level (geostatistics, wavelet and point pattern analyses) suggested some degree of noise in the prevalent NW-SE distributions toward other directions, especially to the orthogonal NE-SW direction. Whereas long bones can roll orthogonally to the main direction of the flow (Voorhies, 1969), noise in the main directional trend at assemblage level may indicate multiple depositional processes, or secondary reworking post-depositional processes. Moreover, the relatively high average density of preserved elements ( $24/m^2$ ) occur in small, well defined clusters (Figs. 2f,e, 4 and 6a). Such spatial aggregation of taphonomic elements may be the result of a combination or the sum of different taphonomic processes (Fernández-López et al., 2002). On the other hand, the formation of gaps in the spatial distribution and clusters of elements in correspondence with topographic depression may as well be associated with lag deposits (Petalglia and Potts, 1994). This is likely to happen on top of rippled surfaces or small dunes in the channel-belt. However, there is no evidence of such structure at TSR.

## 5.2. Differential preservation

According to the evolutionary and systemic theory of taphonomy, taphonomic alteration is not only conceived as a destructive process, but it also has positive effects with the preservation and creation of new taphonomic groups. In this sense, the differential destruction (or taphonomic sieve) of taphonomic enti-

ties is just a particular case of taphonomic alteration, as it is the differential modification that gives rise to selective preservation (Fernández-López, 2006). Intrinsic and extrinsic taphonomic factors determine the differential preservation of taphonomic entities. In this study we integrated our spatial taphonomic approach with a preliminary study of the differential preservation of fossil elements.

In the BM4 class of mammals, the relatively high abundance of skeletal elements belonging to the Voorhies Groups I/II, II and II/III (Fig. 10b) suggests minor winnowing of the assemblage, with preservation of the densest elements that are above the threshold of transportability (Behrensmeyer, 1988). Indeed, skeletal elements in the Voorhies Group I (ribs, vertebrae, sacrum, sternum) tend to be transported more easily by saltation or flotation in relatively low-energy currents (Voorhies, 1969). The under-representation of the Voorhies Group III (crania and complete mandibles) in the BM4 class is balanced by the high occurrence of cranial elements in the Group II/III (rami of mandibles and maxilla fragments). Thus, the distribution in Fig. 10b suggests, more than the taphonomic sieve of the Voorhies Group III, a higher fragmentation rate of cranial elements in the BM4 class of mammals (*Equus*, *Bison*, *Praemegaceros*). On the other hand, the Voorhies Group III is better represented in the BM classes 2 and 3, which include smaller mammals, i.e., *C. etruscus*, *U. etruscus* and medium-sized cervids. The presence of better preserved carnivore cranial elements, as well as the presence of a partial articulated skeleton of a wolf-sized carnivore, would suggest an autochthonous or paraautochthonous assemblage (Behrensmeyer, 1988).

Although excluded from the Voorhies Group analysis, it is worth noting the presence of several mostly complete skeletal elements of Elephantidae (e.g., ribs, scapula, humerus and several articulated carpal, metacarpal and phalanges) with different FTI values, comparable to elements of the Voorhies Group II and III (Frison and Todd, 1986). Their distribution suggests that the assemblage was winnowed of the elements with highest FTI, which are comparable to elements of the Voorhies Group I. This is also the case for the other excluded megaherbivore, the rhinocerotid *Stephanorhinus*, which is represented by several teeth and limb bones.

Overall, the very high teeth/vertebra ratio (7.8) also supports the hypothesis of a lag, winnowed assemblage. Moreover, the actual presence of a high number of limb and undetermined bone fragments, together with complete appendicular and axial elements (Fig. 10c) supports also some degree of sorting (taphonomic sieve) of the smallest, cancellous fragments. Segregation of axial elements from epiphyses and shafts has been observed even in low-energy fluvial environments (Domínguez-Rodrigo et al., 2017).

On the other hand, as noted earlier, the conspicuous presence of articulated specimens in the TSR fossil assemblage does not necessarily suggest an autochthonous deposition, since articulated bones may as well show a great hydraulic transport potential (Coard, 1999; Coard and Dennell, 1995). Nevertheless, it is worth noting that the distribution of articulated units at TSR shows a significant presence of appendicular elements over axial ones (Fig. 10d). Thus, the under-representation of ar-

ticulated axial elements also indicates a winnowed, lag assemblage formed by the densest and most resilient elements, with sieve and transport of part of the lighter and more cancellous elements. However, carnivore ravaging alike tends to eliminate or at least lead to under-representation of those skeletal elements (the less dense, axial elements) in the transport group most prone to be transported by water (Domínguez-Rodrigo et al., 2012; Voorhies, 1969). Interestingly, a preliminary analysis of the bone breakage patterns suggests that carnivores had some active role in the modification and possibly in the accumulation of bones at TSR (Fig. 2e; Konidaris et al., 2015).

In conclusion, considering the results of our spatial taphonomic analysis, processes of taphonomic dispersion, such as fluvial accumulation processes, would have likely separated and disseminated the most cancellous taphonomic elements, favouring the persistence of taphons constituted by allochthonous elements (Fernández-López, 2006). Carnivores could have likely been primary accumulation agents. However, the recursive anisotropic spatial patterns, at the level of taphonomic elements and at the assemblage level, as well as the clustering pattern in relatively small, dense, aggregations of elements aligned in parallel NW-SE oriented bands, suggest that the TSR deposit resulted from multiple taphonomic dispersion events, with winnowing of less dense, lighter elements and spatial anisotropic re-arrangement of a lag, autochthonous assemblage accumulated over the migrating banks of a NW-SE oriented fluvial system. As suggested by Organista et al. (2017), it is likely for secondary overbank flows to aggregate bones dispersed over the bank surface into topographic depressions, where they accumulate and acquire greater stability.

Noteworthy, both Geo 1 and Geo 2 show fining upward trends and facies sequences similar to those typical of braided rivers (Miall, 1977). In such a sequence, the lower coarser-grained part would represent one or more sets of sinuous-crested medium-scale bedforms (i.e., small dunes) forming by bedload traction in the deeper reaches of channels, whereas the upper muddy part is dominantly deposited by decantation either on top of in-channel or bank-attached emerging bars or in flood plains, occasionally provided with coarse material at high-water stages (Miall, 1982). Therefore, the excavated section can be viewed as the product of cyclical lateral switching of a braided fluvial system.

## 6. Conclusions

Spatial taphonomy is the systemic, multiscale and multi-level study of the spatial properties of taphonomic processes. Indeed, taphonomic alteration processes work simultaneously at different scales, on entities of different levels of organization, from the basic taphonomic elements (bone specimens), to higher level taphonomic groups (taphons) or populations (assemblages). In this study we elaborated on a specific aspect - anisotropy - of the spatial properties of taphonomic processes, investigating an often neglected aspect of the spatial distribution of taphonomic populations.

A multilevel analysis of anisotropy was conducted for the Early Pleistocene fossiliferous locality Tsiotra Vryssi, from the

fluvial Gerakarou Formation of the Mygdonia Basin, Greece. Differential preservation of skeletal elements was also analysed in order to unravel the character and number of depositional processes and the degree of re-elaboration of the TSR fossil record. The results of the analyses suggested repeated taphonomic dispersion processes, with winnowing of less dense, lighter elements and spatial anisotropic re-arrangement of a lag, autochthonous assemblage possibly accumulated over the migrating banks of a NW-SE oriented fluvial system.

We believe that this study contributes towards the development of a referential framework for the spatial taphonomic interpretation of other palaeontological, as well as archaeological, localities.

## Acknowledgements

This research was supported by the European Research Council [ERC StG PaGE 'Paleoanthropology at the Gates of Europe: Human evolution in the southern Balkans' 283503, 2014] and [ERC CoG CROSSROADS 'Human Evolution at the Crossroads' 724703, 2017] awarded to K. Harvati. We are grateful to all the participants in the survey and excavation campaigns that took place in the Mygdonia Basin for their indispensable contribution.

## References

- Aramendi, J., Urielarrea, D., Arriaza, M. C., Arráiz, H., Barboni, D., Yravedra, J., Ortega, M. C., Gidna, A., Mabulla, A., Baquedano, E., Domínguez-Rodrigo, M., 2017. The paleoecology and taphonomy of AMK (Bed I, Olduvai Gorge) and its contributions to the understanding of the "Zinj" paleolandscape. *Palaeogeography, Palaeoclimatology, Palaeoecology* 488, 35–49.
- Baddeley, A., Rubak, E., Turner, R., 2015. *Spatial Point Patterns: Methodology and Applications* with R. Chapman and Hall/CRC, London.
- Balsey, J. R., Buddington, A. F., 1960. Magnetic susceptibility anisotropy and fabric of some adirondack granites and orthogneisses. *American Journal of Science* 258, 6–20.
- Behrensmeyer, A., 1975a. Taphonomy and paleoecology in the hominid fossil record. *Yearbook of Physical Anthropology* 19, 36–50.
- Behrensmeyer, A. K., 1975b. The taphonomy and paleoecology of Plio-Pleistocene vertebrate assemblages East of Lake Rudolf, Kenya. *Bulletin of the Museum of Comparative Zoology* 146, 473–578.
- Behrensmeyer, A. K., 1982. Time resolution in fluvial vertebrate assemblages. *Paleobiology* 8 (3), 211–227.
- Behrensmeyer, A. K., 1988. Vertebrate preservation in fluvial channels. *Palaeogeography, Palaeoclimatology, Palaeoecology* 63 (1), 183–199.
- Benito-Calvo, A., de la Torre, I., 2011. Analysis of orientation patterns in Olduvai Bed I assemblages using GIS techniques: Implications for site formation processes. *Journal of Human Evolution* 61 (1), 50–60.
- Benito-Calvo, A., Martínez-Moreno, J., Mora, R., Roy, M., Roda, X., 2011. Trampling experiments at Cova Gran de Santa Linya, Pre-Pyrenees, Spain: their relevance for archaeological fabrics of the Upper–Middle Paleolithic assemblages. *Journal of Archaeological Science* 38 (12), 3652–3661.
- Bertran, P., Texier, J.-P., 1995. Fabric Analysis: Application to Paleolithic Sites. *Journal of Archaeological Science* 22 (4), 521–535.
- Bevan, A., Conolly, J., 2009. Modelling spatial heterogeneity and nonstationarity in artifact-rich landscapes. *Journal of Archaeological Science* 36 (4), 956–964.
- Boaz, D. D., 1982. Modern riverine taphonomy: its relevance to the interpretation of Plio-Pleistocene hominid paleoecology in the Omo basin, Ethiopia. Ph.D. thesis.
- Boaz, N. T., Behrensmeyer, A. K., 1976. Hominid taphonomy: Transport of human skeletal parts in an artificial fluvial environment. *American Journal of Physical Anthropology* 45 (1), 53–60.

- 1076 Coard, R., 1999. One bone, two bones, wet bones, dry bones: Transport potentials under experimental conditions. *Journal of Archaeological Science* 148  
1077 26 (11), 1369–1375. 1149
- 1078 Coard, R., Dennell, R., 1995. Taphonomy of some articulated skeletal remains. *Transport potential in an artificial environment. Journal of Archaeological Science* 22 (3), 441–448. 1150  
1080 1152
- 1081 Cobo-Sánchez, L., Aramendi, J., Domínguez-Rodrigo, M., 2014. Orientation patterns of wildebeest bones on the lake Masek floodplain (Serengeti, Tanzania) and their relevance to interpret anisotropy in the Olduvai lacustrine floodplain. *Quaternary International* 322–323 (0), 277–284, the Evolution of Hominin Behavior during the Oldowan-Acheulian Transition: Recent Evidence from Olduvai Gorge and Peninj (Tanzania). 1153  
1083 1155  
1084 1157  
1085 1159  
1086 1161  
1087 1162  
1088 1163  
1089 1164  
1090 1165  
1091 1166  
1092 1167  
1093 1168  
1094 1169  
1095 1170  
1096 1171  
1097 1172  
1098 1173  
1099 1174  
1100 1175  
1101 1176  
1102 1177  
1103 1178  
1104 1179  
1105 1180  
1106 1181  
1107 1182  
1108 1183  
1109 1184  
1110 1185  
1111 1186  
1112 1187  
1113 1188  
1114 1189  
1115 1190  
1116 1191  
1117 1192  
1118 1193  
1119 1194  
1120 1195  
1121 1196  
1122 1197  
1123 1198  
1124 1199  
1125 1200  
1126 1201  
1127 1202  
1128 1203  
1129 1204  
1130 1205  
1131 1206  
1132 1207  
1133 1208  
1134 1209  
1135 1210  
1136 1211  
1137 1212  
1138 1213  
1139 1214  
1140 1215  
1141 1216  
1142 1217  
1143 1218  
1144 1219  
1145 1220  
1146 1221  
Miocene Marnoso Arenacea Formation (northern Apennines, Italy). *Sedimentary Geology* 335, 197–215.
- Fernández-Jalvo, Y., Scott, L., Andrews, P., 2011. Taphonomy in palaeoecological interpretations. *Quaternary Science Reviews* 30 (11), 1296–1302.
- Fernández-López, R. S., Fernández-Jalvo, Y., Alcalá, L., 2002. Accumulation: taphonomic concept and other palaeontological uses. In: Renzi, M. D., Alonso, M. P., Belinchón, M., Peñalver, E., Montoya, P., Márquez-Aliaga, A. (Eds.), *Current Topics on Taphonomy and Fossilization*. pp. 37–47.
- Fernández-López, S., 2006. Taphonomic alteration and evolutionary taphonomy. *Journal of Taphonomy* 4 (3), 111–142.
- Fiorillo, A. R., 1988. A proposal for graphic presentation of orientation data from fossils. *Contributions to Geology* 26 (1), 1–4.
- Fiorillo, A. R., 1991. Taphonomy and depositional setting of Careless Creek Quarry (Judith River Formation), Wheatland County, Montana, U.S.A. *Palaeogeography, Palaeoclimatology, Palaeoecology* 81 (3), 281–311.
- Frison, G. C., Todd, L. C., 1986. *The Colby Mammoth Site: Taphonomy and Archaeology of a Clovis Kill in Northern Wyoming*. University of New Mexico Press.
- Giusti, D., Arzarello, M., 2016. The need for a taphonomic perspective in spatial analysis: Formation processes at the Early Pleistocene site of Pirro Nord (P13), Apricena, Italy. *Journal of Archaeological Science: Reports* 8, 235–249.
- Giusti, D., Toureloukis, V., Konidaris, G., Thompson, N., Karkanas, P., Panagopoulou, E., Harvati, K., in press. Beyond maps: Patterns of formation processes at the Middle Pleistocene open-air site of Marathousa 1, Megalopolis basin, Greece. *Quaternary International*.
- Hamilton, N., Rees, A. J., 1970. The use of magnetic fabric in palaeocurrent estimation. In: Runcorn, S. K. (Ed.), *Palaeogeophysics*. Academic, London, pp. 445–464.
- Hill, A., 1976. On carnivore and weathering damage to bone. *Current Anthropology* 17, 335–336.
- Hrouda, F., 1982. Magnetic anisotropy of rocks and its application in geology and geophysics. *Geophysical Surveys* 5 (1), 37–82.
- Hrouda, F., Janák, F., 1976. The changes in shape of the magnetic susceptibility ellipsoid during progressive metamorphism and deformation. *Tectonophysics* 34, 135–148.
- Jammalamadaka, S., Sengupta, A., Sengupta, A., 2001. *Topics in Circular Statistics. Series on multivariate analysis*. World Scientific.
- Jelinek, V., 1981. Characterization of the magnetic fabrics of rocks. *Tectonophysics* 79, 63–67.
- Kaufmann, C., Gutiérrez, M. A., Álvarez, M. C., González, M. E., Massigoge, A., 2011. Fluvial dispersal potential of guanaco bones (*Lama guanicoe*) under controlled experimental conditions: the influence of age classes to the hydrodynamic behavior. *Journal of Archaeological Science* 38 (2), 334–344.
- Konidaris, G. E., Kostopoulos, D. S., Koufos, G. D., V. T., Harvati, K., 2016. Tsiotra Vryssi: a new vertebrate locality from the Early Pleistocene of Mygdonia Basin (Macedonia, Greece). In: XIV Annual Meeting of the European Association of Vertebrate Palaeontologists. Koninklijke Nederlandse Akademie Van Wetenschappen, p. 37.
- Konidaris, G. E., Toureloukis, V., Kostopoulos, D. S., Thompson, N., Giusti, D., Michailidis, D., Koufos, G. D., Harvati, K., 2015. Two new vertebrate localities from the Early Pleistocene of Mygdonia Basin (Macedonia, Greece): Preliminary results. *Comptes Rendus Palevol* 14 (5), 353–362.
- Koufos, G. D., Konidaris, G. E., Harvati, K., in press. Revisiting *Ursus etruscus* (Carnivora, Mammalia) from the Early Pleistocene of Greece with description of new material. *Quaternary International*.
- Koufos, G. D., Syrides, G. E., Kostopoulos, D. S., Koliadimou, K. K., 1995. Preliminary results about the stratigraphy and the palaeoenvironment of Mygdonia Basin, Macedonia, Greece. *Geobios* 28 (Supplement 1), 243–249, first European Palaeontological Congress.
- Kühn, P., Aguilar, J., Miedema, R., 2010. Textural pedofeatures and related horizons. In: Stoops, G., Marcelino, V., Mees, F. (Eds.), *Interpretation of micromorphological features of soils and regoliths*. Elsevier, Oxford, pp. 217–250.
- Lanza, R., Meloni, A., 2006. *The Earth's Magnetism: An Introduction to Geologists*. Springer, Berlin.
- Legendre, P., Legendre, L., 2012. *Numerical Ecology. Developments in Environmental Modelling*. Elsevier Science.
- Lenoble, A., Bertran, P., 2004. Fabric of Palaeolithic levels: methods and implications for site formation processes. *Journal of Archaeological Science* 31 (4), 457 – 469.

- 1218 Lenoble, A., Bertran, P., Lacrampe, F., 2008. Solifluction-induced modifications of archaeological levels: simulation based on experimental data from modern periglacial slope and application to French Palaeolithic sites. *Journal of Archaeological Science* 35 (1), 99 – 110.
- 1219
- 1220
- 1221
- 1222 Lindbo, D. L., Stolt, M. H., Vepraskas, M. J., 2010. Redoximorphic features In: Stoops, G., Marcelino, V., Mees, F. (Eds.), *Interpretation of micromorphological features of soils and regoliths*. Elsevier, Oxford, pp. 129–147.
- 1223
- 1224
- 1225 Liu, B., Saito, Y., Yamazaki, T., Abdelyem, A., Oda, H., Hori, K., Zhao, Q., 2001. Paleocurrent analysis for the Late Pleistocene-Holocene incised valley fill of the Yangtze delta, China by using anisotropy of magnetic susceptibility data. *Marine Geology* 176, 175–189.
- 1226
- 1227
- 1228 Lloyd, C., Atkinson, P., 2004. Archaeology and geostatistics. *Journal of Archaeological Science* 31 (2), 151 – 165.
- 1229
- 1230 Lowrie, W., Hirt, A. M., 1987. Anisotropy of magnetic susceptibility in the scaglia rossa pelagic limestone. *Astro and Planetary Science Letters* 82, 349–356.
- 1231
- 1232
- 1233
- 1234 Lyman, R., 1994. *Vertebrate Taphonomy*. Cambridge Manuals in Archaeology. Cambridge University Press.
- 1235
- 1236 Lyman, R. L., 2010. What taphonomy is, what it isn't, and why taphonomists should care about the difference. *Journal of Taphonomy* 8 (1), 1–16.
- 1237
- 1238 Markofsky, S., Bevan, A., 2012. Directional analysis of surface artefact distributions: a case study from the Murghab Delta, Turkmenistan. *Journal of Archaeological Science* 39 (2), 428 – 439.
- 1239
- 1240 Miall, A. D., 1977. Lithofacies Types and Vertical Profile Models in Braided River Deposits: A Summary. In: Miall, A. D. (Ed.), *Fluvial Sedimentology*. Vol. Memoir 5. Canadian Society of Petroleum Geologists, Calgary, pp. 597–604.
- 1241
- 1242
- 1243
- 1244
- 1245 Miall, A. D., 1982. Analysis of fluvial depositional systems. AAPG, Tulsa, Okla.
- 1246
- 1247 Murphy, C. P., 1986. Thin section preparation of soils and sediments. AB Academic Publishers, Berkhamsted.
- 1248
- 1249 Nash, D. T., Petraglia, M. D. (Eds.), 1987. Natural formation processes and the archaeological record. Vol. 352 of International Series. British Archaeological Reports, Oxford.
- 1250
- 1251 Novak, B., Housen, B., Kitamura, Y., Kanamatsuc, T., Kawamura, K., 2014. Magnetic fabric analyses as a method for determining sediment transport and deposition in deep sea sediments. *Marine Geology* 356, 19–30.
- 1252
- 1253 Organista, E., Domínguez-Rodrigo, M., Yravedra, J., Uribelarrea, D., Arriaza, M. C., Ortega, M. C., Mabulla, A., Gidna, A., Baquedano, E., 2017. Biotic and abiotic processes affecting the formation of {BK} Level 4c (Bed II, Olduvai Gorge) and their bearing on hominin behavior at the site. *Palaeogeography, Palaeoclimatology, Palaeoecology* 488, 59–75.
- 1254
- 1255 Palombo, M. R., 2010. A scenario of human dispersal in the northwestern Mediterranean throughout the Early to Middle Pleistocene. *Quaternary International* 223–224 (0), 179–194.
- 1256
- 1257 Palombo, M. R., 2016. To what extent could functional diversity be a useful tool in inferring ecosystem responses to past climate changes? *Quaternary International* 413 (Part B), 15–31.
- 1258
- 1259 Pante, M. C., Blumenschine, R. J., 2010. Fluvial transport of bovid long bones fragmented by the feeding activities of hominins and carnivores. *Journal of Archaeological Science* 37 (4), 846 – 854.
- 1260
- 1261 Parés, J. M., Hassold, N. J. C., Rea, D. K., van der Pluijm, B. A., 2007. Paleocurrent directions from paleomagnetic reorientation of magnetic fabrics in deep-sea sediments at the Antarctic Peninsula Pacific margin (ODP sites 1095, 1101). *Marine Geology* 242, 261–269.
- 1262
- 1263 Petraglia, M. D., Nash, D. T., 1987. The impact of fluvial processes on experimental sites. In: Nash, D. T., Petraglia, M. D. (Eds.), *Natural formation processes and the archaeological record*. Vol. 352 of International Series. British Archaeological Reports, Oxford, pp. 108–130.
- 1264
- 1265 Petraglia, M. D., Potts, R., 1994. Water Flow and the Formation of Early Pleistocene Artifact Sites in Olduvai Gorge, Tanzania. *Journal of Anthropological Archaeology* 13 (3), 228–254.
- 1266
- 1267 R Core Team, 2017. R: A Language and Environment for Statistical Computing. R Foundation for Statistical Computing, Vienna, Austria.
- 1268
- 1269 Rosenberg, M., Anderson, C., 2011. Passage: Pattern analysis, spatial statistics and geographic exegesis. version 2. *Methods in Ecology and Evolution* 2 (3), 229–232.
- 1270
- 1271 Rosenberg, M. S., 2004. Wavelet analysis for detecting anisotropy in point patterns. *Journal of Vegetation Science* 15 (2), 277–284.
- 1272
- 1273 Schick, K. D., 1987. Experimentally-derived criteria for assessing hydrologic disturbance of archaeological sites. In: Nash, D. T., Petraglia, M. D. (Eds.), *Natural formation processes and the archaeological record*. Vol. 352 of International Series. British Archaeological Reports, Oxford, pp. 86–107.
- 1274
- 1275 Schiffer, M. B., 1987. Formation processes of the archaeological record. University of New Mexico Press, Albuquerque.
- 1276
- 1277 Stacey, F. D., Joplis, G., Lindsay, J., 1960. Magnetic anisotropy and fabric of some foliated rocks from se australia. *Geofisica Pura e Applicata* 47, 30–40.
- 1278
- 1279 Tarling, D. H., Hrouda, F., 1993. *The Magnetic Anisotropy of Rocks*. Chapman and Hall, London.
- 1280
- 1281 Toots, H., 1965. Orientation and distribution of fossils as environmental indicators. In: Nineteenth Field Conference of the Wyoming Geological Association. pp. 219–292.
- 1282
- 1283 Voorhies, M., 1969. Taphonomy and population dynamics of an early Pliocene vertebrate fauna, Knox County, Nebraska. *Contributions to Geology, University of Wyoming Special Paper* 1, 1–69.
- 1284
- 1285 Woodcock, N., Naylor, M., 1983. Randomness testing in three-dimensional orientation data. *Journal of Structural Geology* 5 (5), 539 – 548.